CAPILARY DRIVEN FLOWS IN MICRO-MACHINED OPEN POLYMER MICROCHANNELS

by

Akinjuyigbe A. Alo, B. Tech

A thesis submitted to the Graduate Council of
Texas State University in partial fulfillment
of the requirements for the degree of
Master of Science
with a Major in Engineering
August 2021

Committee Members:

Namwon Kim, Chair

Jitendra Tate

Byoung Hee You

FAIR USE AND AUTHOR'S PERMISSION STATEMENT

Fair Use

Duplication Permission

ACKNOWLEDGEMENTS

All thanks to my supervisor Dr. Namwon Kim for his guidance and support in different aspect of this work for the past three years and few months. It's an honor to learn under a meticulous researcher who has been able to teach to do a quality job. In addition, I would like to say thank you to other committee members Dr. Jitendra Tate and Dr. Byoung Hee You for their corrective feedback contributed towards my thesis work. I highly regard the tremendous effort contributed towards the success of this work.

Lest I forget, I also want to appreciate my sponsors Dr. Akinwumi Odumakinde, Mrs. Alo Pade, Mrs. Bola Parker and the rest of my family members for their financial and morale support during the course of this study.

TABLE OF CONTENTS

Page

LIST OF TABLES

Table **Page**

LIST OF FIGURES

Figure **Page**

ABSTRACT

Wettability and surface roughness have been studied for quite some years now especially in the area of microfabrication, in which more interests have been raised for the use of polymeric materials (acrylic family) for various biomedical applications. This study addresses one of those interests, the effect of fabrication parameters on the surface property of micromachined polymethyl methacrylate (PMMA) by varying the micro-milling parameters including the depth of cut, feed-rate, spindle speed, coolant (air), and the size of drilling bits. From a factor analysis based on experimental results, depth of cut has the highest influence on the surface quality. The wettability study and contact angle measurements showed that different combination of fabrication parameters resulted in varied surface roughness. It was determined that the spindle speed of 20,000 RPM, feed-rate of 800 mm/min, depth of cut of 150 mm, and milling bit of 203μm diameter were optimum fabrication parameters to be used for machining microchannels for the experimental investigation of capillary driven flows. Contact angle measurements shows which of the samples has the highest and lowest value for contact angle thereby determining whether the surface is hydrophobic or hydrophilic. Wenzel model was used to understand the wettability of each of the micromachined surfaces, the lowest contact angle measured was 30.6° at the average surface roughness of 0.84μm, and highest contact angle was 48.2° at the average surface roughness of 1.57μm. Although these results contain some outliers, the optimum fabrication parameters provided the lowest surface roughness with an equivalent contact angle of 39.5°. The other goal of this study is to understand the

relationship between capillary driven flow and wettability parameters (contact angle, surface roughness, and design parameters). An experimental investigation on capillary driven flow was carried out based on a pool of design parameters, the length, width, depth, and aspect ratio of machined microchannels. The results were modeled based on the Washburn equation, which governs the advancing of meniscus with an increase in time. The results showed that the preferred flow rate was achieved at the design parameters such as the aspect ratio of 1.23, 700μm width, and 600μm depth of machined microchannel. Capillary driven flow was relatively fast with test solution mixed with AOT of 0.5g, 1.0g, 2.0g and 3g, except for 3g where the speed is relatively low due to reverse critical micelle concentration.

CHAPTER 1

1.1 Introduction

Microfluidics is an applied science of controlling fluids in a constrained geometry such as a channel smaller than 1 millimeter in at least one dimension [1, 2]. This science has been applied to create devices consuming the reduced quantity of reagents, allowing well-controlled mixing and particle manipulation, integrating and automating multiple assays (known as lab-on-a-chip), and facilitating imaging and tracking of flows for the biochip and immunoassay (see Fig 1.1 – Fig 1.2) [3]. This area encompasses manipulating the volume of fluid ranging from micro to pico-liter scales. Fluid could either be liquid or gas state, provided it runs through microscale channels or fluid-based equipment such as valves and pumps [3]. Polymeric materials can be used for making microfluidic devices using lithographic techniques [4].

One of the most promising applications of microfluidics in biomedical engineering is for the point-of-care (POC) diagnosis [5]. Biological-based cells can be separated from other samples at the preparation stage. Fluidic suspension separation is based on various parameters such as antigenic surface properties, density and electrical charge. This particular separation requires special type of equipment and techniques [5]. However, microfluidics has been able to come up with a solution that either to be integrated into the above techniques or to function as a standalone device to execute the sample preparation [6].

For over a decade, there have been research to improve the POC devices. The market for microfluidics based devices has been on a rise for a decade now especially in the area of pharmaceuticals, intro-diagnostics and medical devices which has led to a high demand in

the researching about the need for POC devices [7]. However, the need for this POC has led to a search for devices that can be used to diagnose for acute myocardial infarction (AMI) using biomarker mainly to detect the ailment [5]. Afterwards, a fluorescence-based assay is used to characterize or quantify the concentration of the biomarker for easy detections. An immunoassay strip is housed by the cartridge on which the fluid sample is dropped and later exposed to a detection light for characterization [8]. However, in this study, a certain alternative to the strip has been investigated. Polymethyl methacrylate (PMMA) make it a suitable material for the strip because of its properties such as hydrophilic surface, low cost, and wettability [9]. The machining technique to be used is the micro-milling process, which is used to fabricate the microchannel. As an engineer, the machining and characterization stages are of great importance in this study.

1.2 Motivation

This project targets to solve issues related with the fluid flow in an open microchannel for the purpose of certain health diagnosis such as vitamin-D test and pregnancy test. From literatures consulted, the paper-based membrane that are mainly used in the diagnosis can be replaced by polymer material based on the following reasons: shelf-life issues, vulnerable to environmental condition, protein inability to bind covalently to nitrocellulose and recyclability after use. Polymers are in numerous types based on the way they are produced, but the main reason for using a particular polymer, called PMMA was because of its low cost, transparency, easy recyclability on a mass scale and good machinability compared with other polymers [10].

1.3 Microfluidics

This field incorporates the fundamentals of automation, fluid mechanics, biology, and chemistry. Microfluidics becomes beneficial to this study based on the ability to control the flow rate of a fluid in a channel, which is fundamental to the research aim. It contains miniaturized plumbing and fluidic control options of solving system incorporation issues for biology and chemistry (see Fig 1.1, Fig 1.2). Certain properties of fluids such as surface tension and viscosity play a big role in the flow rate making it suitable for microfluidic-based devices to be used for biological applications. There is a history of using fluidics as control systems in different devices ranging from logic devices to thrust reversers in aircraft through a research-based program. The thrust reversers research program at the initial stage was not a total success because the scaling properties of the fluid physics prevented miniaturization [11-13].

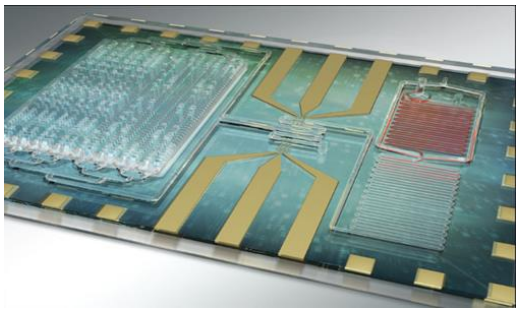

Fig 1.1: Microfluidic sepsis biochip showing microfluidic channel [14].

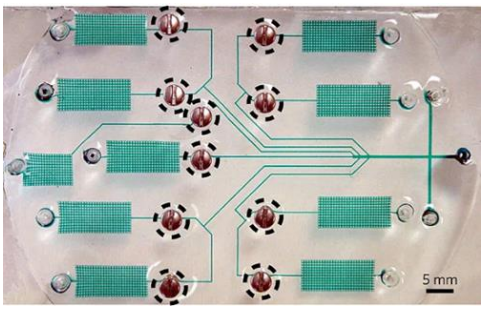

Fig 1.2: Sandwich immunoassay microfluidic device [15].

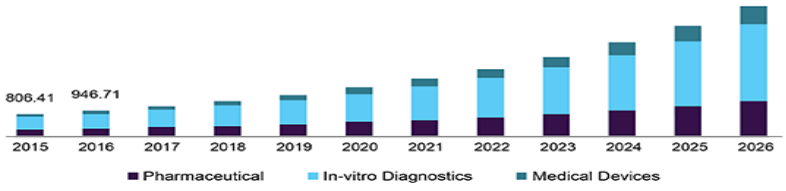

Fig 1.3: Global microfluidics market share by region [7].

A vital property of microfluidics is that the essential physics deviates more rapidly as the size scale decreases. With the advent of microfluidics, force driven effect on fluids can be achieved by capillary forces instead of using pump-driven force, which could incur more cost. Apart from the mentioned benefits of microfluidics in fluid mechanics, other areas such as pharmaceuticals, in-vitro diagnostics such as vitamin-D quantification have seen improvement as a result of microfluidics [16].

The vital fluid physics of a system is discussed in different literatures due to rivalry between various phenomena, which is represented by a series of dimensionless numbers expressing their relative importance. These dimensionless number systems form a type of restriction space for microfluidic physics, which is important for us to understand in order to have knowledge on measuring fluid flow. These numbers in certain cases scale with a distinctive system length such as channel size, and thus designate a significant change in physics. In other cases, the figures are independent of length scale, yet still have important applications such as hydromagnetic, heat transfer and hydrodynamics.

Boundary-driven effect occurs in microchannels that have a definite geometry size and enclosure limiting the fluid flow, which are of specific importance to microfluidic devices because the distinctive geometries of microfluidic devices nearly always have large surface-area-to-volume ratios [17, 18].

1.4 Capillary driven flow

An extensive variability of physical phenomena arises in microfluidic devices, the advantage of which must be judged against competing phenomena. Dimensionless numbers representing the ratios of different physical quantities or properties give a sense for where a system sits in fluidic parameter space. These physical properties include the

speed or velocity, surface tension, viscosity used to measure fluid flow within certain boundary condition such as geometry of the microchannel. The Reynolds number (Re) measures the ratio of inertial forces to viscous forces by describing degree of turbulent or laminar flow [19]. The Deborah number (De) is the ratio of the time it takes for a material to adjust to applied stress or deformations [20]. It is mostly used to characterize the fluidity of materials under certain flow conditions [20]. Weissenberg (Wi) is the ratio of the elastic forces to viscous force. It shows the relationship of stress relaxation time of the fluid and a specific process time [21]. The elasticity numbers along with Re, De, and Wi express the elastic effects observed in fluid flow [22]. The Péclet number (Pe) is a dimensionless number, which is a ratio of advective transport rate to diffusive transport rate relating convection to diffusion [23]. The capillary number (Ca) is the ratio of viscous drag force to surface tension forces acting across the interface between a liquid and gas [17].

Fluid is continuum material, i.e., they occupy all the available space in a given volume without leaving any void, and discrete quantities like mass and force give a way to continuous properties like density and force density that are defined per unit volume. Fluid is known to behave differently in microscale when compared to macroscale because the molecular effects in which the wall-slip becomes pronounced and amplifies certain ordinary continuum effects to the extreme level. However, the liquid flows in microscale can be still explained by continuum hydrodynamics [24]. Continuum hydrodynamics gives a further information on materials especially solids, liquids and gases composing of materials separated by space.

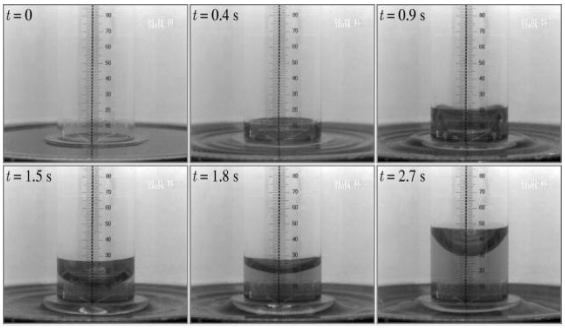

Fig 1.4: Capillary Driven Flow measured in a tube under gravity condition in drop tower Bremen [25].

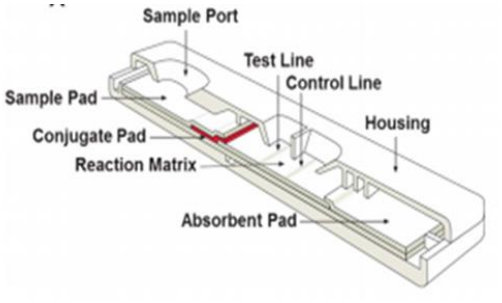

Fig 1.5: Lateral Flow assay device nomenclature [26].

Fig 1.6: Vitamin-D cartridge.

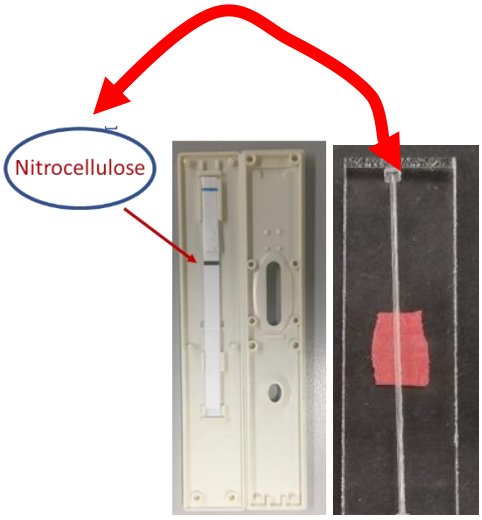

Fig 1.7: Replacing nitrocellulose with PMMA microchannel.

For the purpose of this study, capillary driven force will be used for driving the fluid, which requires us to understand the concept of measuring fluid flow, a type of mass transport (see Fig 1.4). Capillary forces can be used to manipulate and transport fluids with free surfaces, which is the surface subject to zero parallel shear stress such as interface between two homogenous fluids. Capillary driven flow in a microchannel is a result of capillary action

at fluid interface (i.e., gas-liquid-solid interface) without using a mechanical or electrical micro-pumps [27]. The gradients of surface tension force influencing flow field in a microchannel is created by the adjustment of contact angles through surface wettability (i.e. hydrophobicity or hydrophilicity) [28].

Flow rate of the fluid in a microchannel is directly proportional to the hydrophilicity of the microchannel surface since the capillary force is the driving force of the flow. In equilibrium, free surfaces are determined by a balance of interfacial forces of attraction between the molecules of liquid and air, also known as surface tension at the interface of two fluids. Modifying interfacial energies, however, disrupts the balance of interfacial forces between molecules of liquid and air, and causes motion [28, 29]. Broadly speaking, the capillary driven flow has been achieved via two strategies, either by modifying the solid-liquid surface tension, or by inducing a gradient in the liquid-gas surface tension [30].

1.5 Fabrication

Different fabrication techniques have been used for electronic or biomedical applications such as micro laser machining and micro electrical discharge machining. Mechanical micro-milling is one of the techniques for fabricating micro scale parts. It involves the mechanical interaction of a sharp tool with the workpiece material leading to internal material breakage and a removal of useless part of a workpiece in the form of chips [31]. The scale at which micro-milling process operates is entirely different from that of macro-milling machine. For the purpose of this research, micro-milling will be considered. It allows the production of three-dimensional components using various materials including polymers, metal, non-metals, and composites in different engineering applications [32].

Cutting is made effectively by the forces in micro-milling process, which is characterized

by shearing and ploughing effects [33]. The quality of micro-milled part has been influenced by a number of parameters such as the spindle speed, depth of cut, size of the tool diameter, coolant, and cutting temperature [34]. From literatures, the depth of cut, spindle speed and feed-rate are the main parameters that control micro-milling operations. The following requirements must be met for machining operation, high static and dynamic stiffness of the tool to be used for high thermal stability, feed drivers and control system with high accuracy, and fast response time associated with a computer numerical control (CNC) machine. During the operation, the axes responsible for feed and depth of cut must be driven preferably by linear motors with an accuracy of approximate 0.1μm [35].

1.6 Background of research and statement of problem

The main drive for this research is associated with the challenges experienced when using nitrocellulose such as the vulnerability to the environmental condition, protein inability to bind covalently to nitrocellulose, and reduced recyclability after the one-time use. Nitrocellulose has been used for the lateral flow assay (LFA) to quantify the concentration of reagents in a fluid. LFA is also known as lateral flow immune assay, which has four subdivisions, namely reservoir, nitrocellulose membrane, conjugate pad, and sample pad (see Fig 1.5). A year back, our research group suggested that certain advancements might replace the nitrocellulose membrane with polymers. Several studies have been carried out on PMMA as a material to be used for biomedical applications based on its physical and mechanical properties [27]. Its results were remarkable allowing a capillary flow rate of 16 mm/s using a polymer chip that was fabricated by laser ablation technique.

1.7 Aim of the Research

The sole aim of this research work is to replace nitrocellulose with PMMA after surface

modification using a micro-milling machine and to investigate parameters that facilitate capillary driven flow to be used for lateral flow assay (see Fig 1.6 – 1.7). Along with the sole aim of the research work, there are certain goals that this study is targeting as follows:

- To produce rough surface that will be helpful retaining fluids on a polymer surface,
- To identify the core parameters responsible for the targeted surface roughness,
- To determine if there is any relationship between fabrication parameters and surface roughness,
- To control the rate of capillary driven flow by varying the machining parameters such as the depth of cut, feed rate, spindle speed, and coolant selection of either compressed air or oil lubricant,
- To determine the core parameters that affect surface roughness by employing different mathematical models and statistical analysis, and
- To determine significant parameters (e.g., contact angle, surface tension, viscosity, time, and aspect ratio) responsible for the capillary driven flow using Washburn model.

CHAPTER 2

2.1 Literature review

Capillary driven flow has been of great interest for the microfluidic devices due to the fact that there is no need for an external pump to propel the fluid when compared to other microfluidic devices that require an external force for propulsion [6]. For the purpose of this study, capillary force will be the main determinant responsible for the movement of the fluid in a microchannel. Other parameters that aid the capillary driven flow include surface tension, viscosity, geometry, and contact angle [36]. For the purpose of this study, a hydrophilic surface is preferred to facilitate the capillary driven flows. Another factor influencing the capillary force effects is surface tension, a natural force acting on the free surface of liquid, and it generates capillary pressure when the liquid contacts solid surface in a capillary [36].

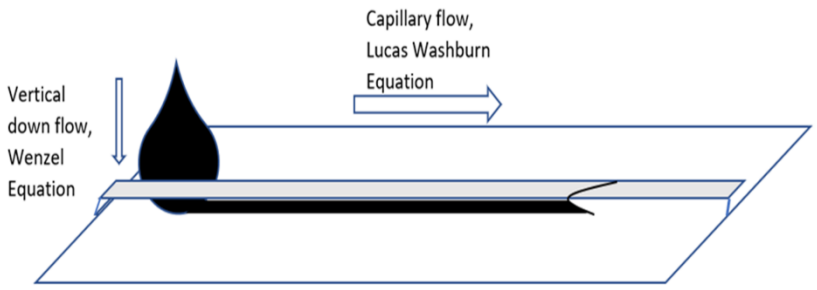

Fig 2.1: Capillary flow in a microchannel.

In a miniaturized microfluidic system, the surface tension becomes dominant over the body force, which is important for microfluidic actuations [37]. This shows that the capillary forces in microfluidics are important as a result of the contact among gas, liquid and solid interfaces [38, 39]. Molecules of liquid are held by cohesive forces whereas the cohesive forces surrounding each of the molecule are balanced by the forces between the molecules

[40]. Surface tension comes to play when there is a decrease in surface energy as a result of a decrease in surface area (see eq. 2.1). The physics behind is that the cohesive forces at the edge of a liquid with neighboring molecules are greater than the interaction with air molecules [41]. Therefore, the liquid molecules at the interface experience a pulling effect.

$$\gamma = {}^{dG}/_{dA} \qquad \text{eq. 2.1}$$

where dG is the change in energy (N·m), dA is the change in area (m^2), and γ is the surface tension or surface energy (N/m).

On a microscale, capillary forces are critical in the sense that surface tension increases the pressure in a bubble trapped in a capillary [42, 43]. Also, it is responsible for increased pressure for pushing liquid into an empty non-wetting capillary. The relationship between surface tension and pressure is represented by Laplace equation (see eq. 2.2).

$$\Delta P = \gamma C \qquad \text{eq. 2.2}$$

where C is the curvature of the liquid surface and ΔP is the change of pressure. Different formulas have been used to determine the curvature depending on the capillary shape [36]:

$$C = \frac{2}{R} \qquad \text{eq. 2.3}$$

$$C = \frac{1}{R_1} + \frac{1}{R_2} \qquad \text{eq. 2.4}$$

where R is the curvature radius for the liquid in a circular capillary, and R_1 and R_2 are the curvatures in a non-circular capillary. In this study, the Lucas-Washburn equation (see eq. 2.5) will be used to determine the capillary flow rate, which will be discussed in subsequent chapter of the writeup.

$$X^2 = \frac{\gamma R cos\theta}{2\mu} t \qquad \text{eq. 2.5}$$

where X is the meniscus position, θ is the contact angle, t is the time, and μ is the viscosity of fluid.

2.2 Pmma Materials

A low cost thermoplastic polymer, PMMA have been used for various applications [44-46]. It is a commercial acrylic polymer and available under several trade names known as Plexiglas® and Acrylite®. Certain properties of this polymer such as high transparency and compatibility with human tissue make it suitable for prosthetics and microfluidics. It is formed through emulsion polymerization of methacrylic acid. In the first half of 20th century, PMMA was thought to be an actactic polymer meaning the substituents of the molecular chain alternatives [44-47] (see fig 2.2A and 2.2B).

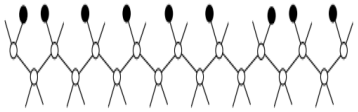

Fig 2.2A: Atactic structure of molecular chain [48].

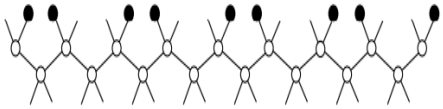

Fig 2.2B: Syndiotactic structure of molecular chain [48].

PMMA is processed using injection molding or extrusion for mass production at melting temperature ranging from 200-230 °C [46, 47]. A pendent group is formed when a cluster of atoms bonds is detached from the backbone of the polymer chain. This group is responsible for the interesting properties in PMMA. The pendent group blocks the crystallization as a result of the inability of the molecules to get close to form crystalline bond leading PMMA to be amorphous. The slip could be eliminated among polymer chains

when the pendent groups snag on adjacent group [44]. This makes PMMA to have the increased brittleness, rigidity, high glass transition, and little mold shrinkage.

Degradation of optical and mechanical properties caused by UV light exposure is minimal with PMMA because it absorbs only trace amounts of light and UV radiation due to its transparency. The small dose of absorbed UV cannot breakdown molecular bonds, which makes it suitable for the long-term weather resistance. Its scratch resistance is high compared to other polymers, especially polycarbonate, however, low when compared to glass. Therefore, there is still a need for protective coatings [46, 47].

PMMA has a wide range of applications especially when low cost, transparency and weather resistance are required. Some examples of these applications are housings for headlights and taillights on passenger automobiles, illuminated signs, and streetlamps. It has also been used widely for the aircraft window as a glass replacement because of its low density and superior toughness [44, 47]. Furthermore, there are certain advantages like thermo-plasticity, transparency, easy recycling on a mass scale, and a minimum manufacturing time that allow PMMA a best fit to replace nitrocellulose.

2.3 Fabrication method

Micro-electrical discharge machining, micro laser machining, and micro-milling are used to fabricate micro-scale parts based on different engineering materials [34]. Micro-milling is widely used for fabricating micro-parts with three dimensional surfaces [49]. It is a flexible technique that allows high precision milling, although miniature precision milling machines could be expensive [50].

The micro-milling involves the removal of substrate material. The process parameters such as the spindle speed, depth of cut, and feed rate [50] are important for this fabrication

process. Different types of work have been carried out using the micro-milling process specially to show the relationship between input parameters (spindle speed, feed rate, and depth of cut) and output parameters (quality of milled surface i.e., surface roughness). One of the works carried by Biermann analyzed the machinability of hardened tool steel using three different types of coated carbide tools. The experimental study take account of the following process variables; feed per tooth, axial depth of cut, radial depth of cut, and feed per tooth while the process outputs were machining forces, tool wear, surface quality, and material removal rate [51]. Their results showed that deflection and vibration must be decreased to obtain a good surface quality.

Another researcher, Filiz et al. studied the slot milling of pure copper using tungsten carbide cutting tools. They investigated the cutting forces, surface roughness, tool wear, and burr formation under various cutting speeds and feed rates to analyze the effects of parameters on the process outputs [52]. They realized that minimum chip thickness caused irregular variations in cutting force at low feed rates. An experimental study of Natarajan et al. revealed that the low feed rate yielded better surface finish, and the spindle speed has no significant effect on the surface roughness [52]. However, in most study carried out on micro-milling, the parameters such as cutting forces, surface roughness, tool wear, and burr formation have been an important consideration in material removal process to meet the dimensional and surface quality requirements.

2.4 Taguchi method

In 1950s, Dr. Genichi Taguchi was known as “the father of Quality Engineering” who initiated a concept of off-line quality control techniques known as Taguchi parameter design [53, 54]. Off-line quality control techniques are those activities performed during

the design and development phases [55]. The concept is based on the fractional factorial design and categorized into two processes: reducing the process or product variations and designing robust and flexible processes adaptable to environmental conditions [53, 56]. “Robust” in this case means the process or product performs consistently and relatively insensitive to factors that are difficult to control.

Two important tools used in the parameter design are orthogonal arrays and signal-to-noise (S/N) ratios [57]. Orthogonal arrays have a balanced property in which every factor setting occurs the same number of times for every setting of all other factors in the experiment [54]. Orthogonal arrays allow researchers to analyze many design parameters simultaneously and estimate the effects of each factor independent of other factors. Taguchi’s optimization technique is a unique and powerful tool that permits optimization with the minimum number of experiments. Experimental design based on Taguchi reduces the cost, improves the quality, and provides the robust design solutions [34]. Other approaches used in the process development include build-test-fix method, design of experiments, and full factorial design [34].

General procedures involved in Taguchi method include identifying the main functions and side effects, identifying the noise factors, testing condition and quality characteristics, identifying the objective function to be optimized, identifying the controlling factor and their levels, selecting a suitable orthogonal array and constructing matrix, conducting matrix experiments, examining the data, predicting optimum control factors levels, and conducting verification experiments [53]. Analysis of variance (ANOVA) can be used to evaluate the response magnitude of each parameter in the orthogonal experiment. It is used to identify and quantify the sources of different trial resulted from different trial runs. Basic

property of ANOVA includes the total sums of squares equal to the sums of the squares of deviations of all the condition parameters and error components [58].

Different models were used for the surface roughness determination based on the physical model (see eq. 2.6) with a linearized model (see eq. 2.7) for statistical approach in order to evaluate the fabrication parameters that has the highest significance on the roughness [59]. Eq. 2.6 stated the physical model for surface roughness where R_a is the surface roughness, D_f is the spindle speed (RPM), V is the feed rate (mm/min), a_p is the depth of cut (μm), f_2 is the diameter of drilling bit (μm), a_0 is the surface roughness constant, a_1 is the number of speed combinations, a_2 is the number of feed combinations, a_3 is the number of depth of cut combinations, and a_4 is the number of drilling bits.

$$R_a = a_0 . D_f^{a_1} . V^{a_2} . a_p^{a_3} . f_2^{a_2} \qquad \text{eq. 2.6}$$

$$lgR_a = lga_0 . a_1 lgD_f . a_2 lgV . a_3 lga_B . a_4 lgf_2 \qquad \text{eq. 2.7}$$

2.5 Wettability studies of solid surface

Wettability is the property of liquid to spread on a solid surface. The liquid deposited on the surface has the tendency to spread until cohesion (internal forces) of the liquid, the gravity forces and capillary (surface tension) forces are in balance, and an equilibrium state is reached [41]. The main parameter for describing a wetting behavior of functional surfaces is the contact angle (CA).

2.6 Contact Angle

For an effective wettability study, three models including Wenzel, Cassie, and Young's models have been considered. Young's model as follows

$$S_G = S_L + L_G \cos\theta \qquad \text{eq. 2.5}$$

where S_G is the solid-gas surface tension, L_G is the liquid-gas surface tension, and S_L is the

solid-liquid interfacial tension. The Young's contact angle (CA) is formed between the tangent to the liquid-gas interface and the surface itself at the contact point of three phases. It can also be denoted as an ideal CA or intrinsic CA, if the drop size is sufficiently large and the effect of line tension is negligible [60]. Based on the wettability of ideal solid surfaces by water drops can be classified into two states by the theoretical threshold, θ_y = 90°:

If $\gamma_s < \gamma_{sl}$, then 90° < θ_y < 180° intrinsic hydrophobic (water-repelling) [30]

If $\gamma_s > \gamma_{sl}$, then 0° < θ_y < 90° intrinsic hydrophilic (water-attracting) [61]

Common surfaces are usually rough and chemically heterogenous. There are two kinds of contact angles; the actual contact angle between the tangent to the liquid-air interface and the solid surface [62] and the apparent contact angle that is directly measured and defined as the angle between the tangent to the liquid-air interface and line that represents the nominal solid surface as seen macroscopically [62].

From thermodynamics point of view, the Gibbs free energy curve of a real wetting system as a function of θ_{ap} exhibits multiple local energy minima because of roughness and chemical heterogeneities of the solid phase. The range is called the contact angle hysteresis with the highest and lowest observed θ_{ap} referred to as advancing and receding contact angles, θ_{aca} and θ_{rca}, respectively.

$$CA_{hysteresis} = \theta_{aca} - \theta_{rca} \qquad \text{eq. 2.6}$$

Depending on the behavior of liquid droplet on a rough solid surface, two classical and well-established wetting regimes can be distinguished. When the liquid completely covers the surface, the situation is called homogeneous wetting and can be described by

the Wenzel equation:

$$\cos\theta_w = r\cos\theta_y \qquad \text{eq. 2.7}$$

where the Wenzel CA θ_w is equal to θ_{ap} and r is the roughness ratio, which is defined as the real solid surface area related to its projected area. A detailed consideration leads to the following conclusion concerning the theoretical relationship between CA and roughness:

Ideal smooth surface (r = 1): $\theta_w = \theta_y$

Hydrophobicity (θ_y > 90°): increase of r results in weaker wetting ($\theta_w > \theta_y$)

Hydrophilicity (θ_y < 90°): increase of r results in stronger wetting ($\theta_w < \theta_y$)

Thus, increasing roughness enhances the intrinsic wetting properties in both directions. In case of the heterogenous wetting state, air cavities are situated in the roughness structures below the liquid phase. For this situation, the equation developed by Cassie and Baxter becomes valid;

$$\cos\theta_m = x_1\cos\theta_{y_1} + x_2\cos\theta_{y_2} \qquad \text{eq. 2.8}$$

where x is the area fraction characterized by the given chemistry and subscripts 1 and 2 indicating two different surface chemistries. The Cassie-Baxter approximation is derived from Wenzel equation in combination with Cassie equation that is popularly used for smooth, but chemically heterogeneous solid surface.

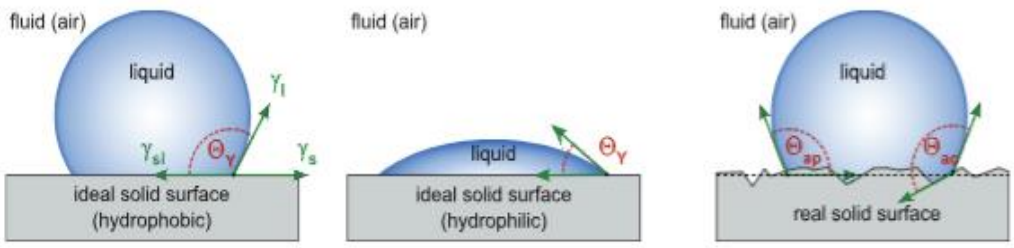

Fig 2.3: (A) Liquid droplet on an ideal solid hydrophobic surface. (B) Liquid droplet on an ideal solid hydrophilic surface. (C) Liquid droplet on a real solid surface [63].

2.7 Surfactant

Surfactant molecules are dual in nature i.e., this property originates from their amphiphilic structure, which comprises of the head (hydrophilic) and tail (hydrophobic) groups. The molecule attacks the interface between two immiscible surfaces thereby decreases the interfacial interaction between two surfaces. Surfactants are widely used in microfluidic systems because they reduce surface tensions.

They are classified in four categories namely, anionic surfactants, nonionic surfactants, cationic surfactants, and amphoteric surfactants. Anionic surfactant contains a negatively charged head and they are mostly used in sandstone reservoirs because of their low cost and good reservoir properties. Cationic surfactant contains a positively charged head. Cations are sometimes used in carbonates to alter the wettability, but they are costly. Non-ionic surfactant has no head group. They are mainly used as co-surfactants because they are less sensitive to salinity, cheap and improve the system phase behavior by increasing the oil solubilizing capacity. Amphoteric surfactant contains both positive and negative charges. Bio surfactants are surfactants of biological origins like bacteria or yeast. They are attracting much attention recently because of their lower toxicity and high salinity. For the purpose of this study, AOT (dioctyl sulfosuccinate sodium salt) is the surfactant to be

used because it is anionic, biocompatible, readily available, and less expensive compared to other types of surfactants.

Surfactants at low concentrations exist as isolated molecules. As the concentration of the surfactant increases, the molecules rearrange such that hydrophilic portion is in the water phase and the hydrophobic portion is in the oil phase [62, 64, 65]. This will reduce the interfacial tension significantly. When the surfactant concentration reaches the critical micelle concentration (CMC), molecules will start aggregating together and forming structures called micelles [66, 67].

2.8 Mobility parameter

Flow rate in an open microchannel can be modeled based on the force balance, which is represented by Washburn equation. Fluid flow in the microchannel was driven by two forces acting against each other, the driving force was caused by the capillarity while the opposing force was by viscous friction. The derivation of capillary force is as follows

$$x^2 = K * t \qquad \text{eq. 2.12}$$

where x is the position of advancing meniscus (mm), K is the mobility constant, and t is the time of travel for the capillary flow (sec). Cross section of the rectangular channel thus corresponds to

$$-(w/2) \leq y \leq +(w/2) \qquad \text{eq. 2.13}$$

$$0 \leq z \leq D \qquad \text{eq. 2.14}$$

where w is the width of microchannel (mm), D is the diameter of microchannel (mm), y is the extrapolated width (mm), and z is the extrapolated diameter (mm).

Driving force caused by the effect of the capillary pressure is

$$F_\gamma = -\frac{dE}{dx} \qquad \text{eq. 2.15}$$

where *dE* is the change of energy (N·m), *dx* is the change of meniscus position (m). Those forces are balanced after a certain period of time. Several assumptions were made based on this model,

- The liquid flow was restricted by the walls of the channel.
- The depth of microchannel was constant from the entry to the exit at the meniscus level.
- Volume and shape changes were resulted as the liquid was filling constantly from entry.

CHAPTER 3

3.1 Materials and methods

For this experimental study, two main experimental steps were carried out to achieve the capillary driven flow in a microchannel. The first experiment involves the use of Taguchi method for the design of experiments in order to create a pool of machining parameters for the microchannel fabrication. The second experiment is to carry out the capillary driven flow experiment. In the first experiment, the different fabrication parameters were varied to see their effects on the surface roughness. The aim for the first experiment was to find optimized machining parameters for engineered polymer surface enhancing the capillary driven capability by measuring the surface roughness and contact angle that determine the hydrophilicity or hydrophobicity of a surface.

A polymer substrate with a square pocket at each corner was designed by using Fusion 360 (version 2.0.5818, San Rafael, CA). Each of the 10 mm × 10 mm square pockets had different depths of cut, but the same depth of 150μm (see Figs. 3.1 and 3.2). As a result of this, Tabl**e 3.1** shows the list of fabrication parameters and output parameters. The fabrication parameters include the depth of cut, spindle speed, feed rate, and the diameter of milling bit. The output parameters are the surface roughness and contact angle.

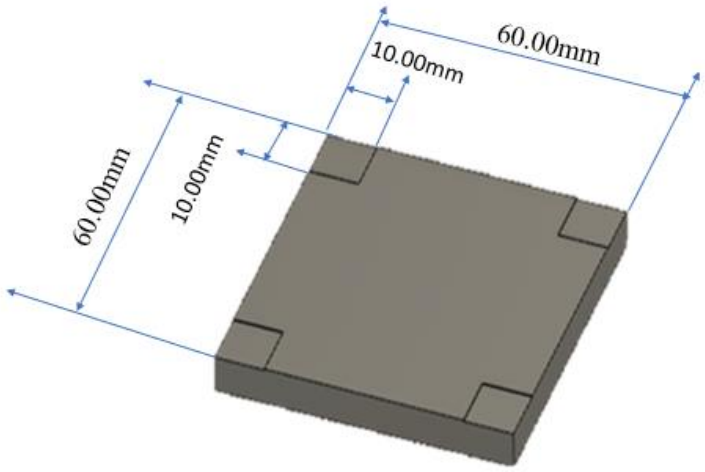

Fig 3 1: A 2D schematic view of the pockets at the corner of a PMMA plate.

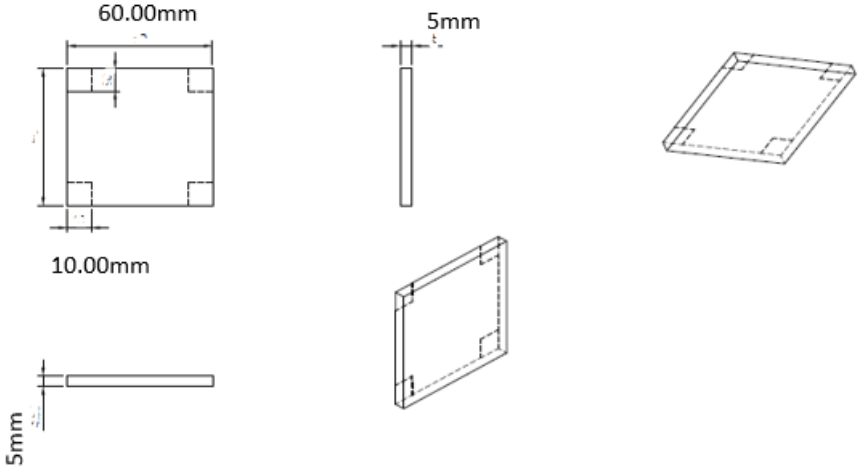

Fig 3 2: Orthographic projection view of the fabricated pockets of the PMMA plates.

54 different combinations of the spindle speed, depth of cut, and feed rate were varied by fixing two fabrication parameters such as the spindle speed of 10,000 RPM and milling bit of 101µm diameter while variating the other fabrication parameters such as the feed rate

and depth of cut, in a repetitive manner. For the following set of 9 samples, the spindle speed was increased to 15,000 RPM and 20,000 RPM while fixing the milling bit diameter. Afterwards, the same process has been repeated for the next 27 samples by increasing the milling bit diameter to 203µm.

Table 3.1: A Taguchi table Showing Different Micro-Milling Combinations

Speed (rpm)	Feed (mm/min)	DOC (mm)	Drilling bit (µm)	Surface roughness (µm)	Contact Angle (deg)
10000	300	50	101	1.87	41.90
10000	600	75	101	1.94	43.00
10000	800	150	101	1.74	44.70
10000	300	75	101	1.56	41.80
10000	600	50	101	1.65	41.70
10000	800	150	101	1.53	44.30
10000	300	75	101	1.61	40.70
10000	600	150	101	2.00	36.30
10000	800	50	101	1.82	39.10
15000	300	50	101	1.84	36.90
15000	600	75	101	1.91	34.20
15000	800	150	101	1.47	40.20
15000	300	50	101	2.27	36.80
15000	600	75	101	1.60	32.70
15000	800	150	101	1.94	35.90

15000	300	50	101	1.44	40.60
15000	600	75	101	2.58	38.20
15000	800	150	101	2.13	37.80
20000	300	50	101	2.22	34.30
20000	600	75	101	2.29	39.10
20000	800	150	101	2.08	34.10
20000	300	50	101	2.31	38.40
20000	600	75	101	2.20	41.10
20000	800	150	101	2.44	36.10
20000	300	50	101	1.80	38.10
20000	600	75	101	1.88	36.80
20000	800	150	101	1.95	34.20
10000	300	50	203	0.54	44.90
10000	600	75	203	0.44	48.20
10000	800	150	203	0.48	41.90
10000	300	50	203	0.65	39.90
10000	600	75	203	0.93	38.90
10000	800	150	203	0.65	34.90
10000	300	50	203	0.59	39.20
10000	600	75	203	0.62	34.70
10000	800	150	203	0.66	34.80
15000	300	50	203	0.64	33.20
15000	600	75	203	0.66	33.80

15000	800	150	203	0.99	33.20
15000	300	50	203	0.79	33.30
15000	600	75	203	0.61	33.00
15000	800	150	203	1.08	38.00
15000	300	50	203	0.40	35.80
15000	600	75	203	0.91	34.60
15000	800	150	203	0.61	35.60
20000	300	50	203	0.65	35.20
20000	600	75	203	0.67	37.80
20000	800	150	203	1.48	36.20
20000	300	50	203	0.64	33.80
20000	600	75	203	0.78	31.20
20000	800	150	203	0.79	36.70
20000	300	50	203	0.70	37.70
20000	600	75	203	0.62	31.20
20000	800	150	203	0.84	30.70

The physical and chemical properties of substrate materials were characterized, which enables a material to be used in various practical applications. For the purpose of this research work, different characterization equipment such as surface profiler (P-7, KLA Tencor, Milpitas, CA) and contact angle and surface tension measurement machine (FTA1000 series, Falcon, First Ten Angstroms, Inc., Portsmouth, VA), measuring microscope (MM-800, Nikon Corp., Kawasaki, Japan), and Quadra-Check Digital Readout

(Heidenhain Corp., Traunreut, Germany) were used.

The surface profiler provides information of the surface topography while the contact angle and surface tension measurement machine provide information about certain physical properties such as contact angle, surface energy, and wetting tension. The contact angle and surface measurement machine enable the researcher to determine the hydrophobicity of the surface. A surface profiler consists of two parts, sample stage and a detector. Sample stage that simultaneously house the sample and move the sample to the point of measurement while the detector determines the surface topography.

There are two types of surface profilometers, which are stylus and optical types. Stylus profilometers use a probe to detect the surface by moving physically with the probe to get the surface roughness while optical profiler uses the reflected light to detect the surface roughness. For a stylus profiler, it gives a feedback loop that monitors the force from the sample pushing up against the probe as it scans along the surface. A feedback system is used to keep the arm with a specific amount of torque known as “setpoint”. The changes in the Z position of the arm holder can be used to reconstruct the surface. Stylus profilometry requires force feedback and physically touching the surface, so it is extremely sensitive and provides high Z resolution.

Fig 3.3: MM – 800, Nikon Corp measuring microscope

Fig 3.4: Quadra-check Digital Readout

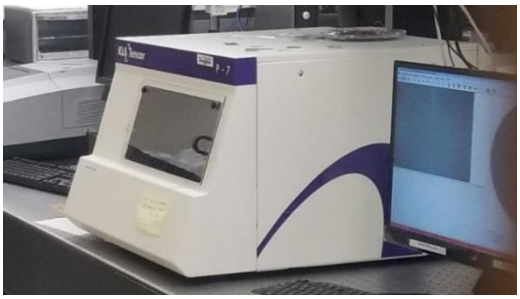

Fig 3.5: P-7, KLA Tencor, Surface Profiler

3.2 Micromilling machine setup

PMMA was purchased from McMaster and Regal Plastics for the purpose of this experiment. The sample was cut into a dimension of 60 mm × 60 mm from a PMMA slab of dimension 140 mm × 140 mm using a laser cutting system (Universal Laser Systems, HD-1390, Cerritos, CA). Afterwards, computer-aided manufacturing (CAM) function of the software, Fusion 360 (version 2.0.5818, San Rafael, CA) was used to generate G-code for milling process. The PMMA substrate was mounted on the three-headed jaw of the micro-milling machine (see Fig 3.6) before the milling was automated from the computer

using CNC software (Mach3, MACH, Livermore, ME) of a 5-axis milling machine (Minitech, Norcross, GA).

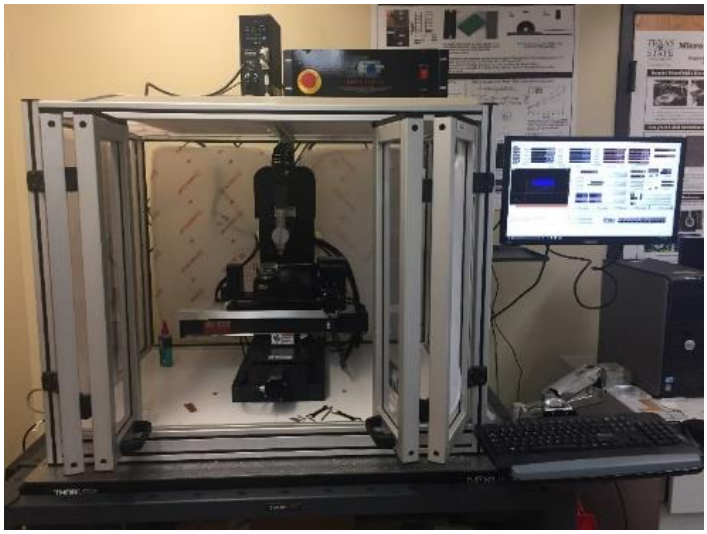

Fig 3.6: Micro-milling machine setup

Milling bits (Performance Micro Tool PMT, Livermore, WI) of two diameters; 0.101 mm (Part Number TR-2-0040-S TRACE 41739) and 0.203 mm (Part Number TR-2-0080-S TRACE 41895) were used. The milling took an average of 4 hours with a smooth edge surface at the edges of the squared cut PMMA. The machined surface of samples was cleaned using deionized water (DI water) and Isopropyl alcohol (IPA). Afterwards, the cleaned samples were subjected to mega-sonic cleaning using an ultrasonic machine (CPXH 2800, Branson, Danbury, CT) for 60 seconds.

3.3 Contact angle measurements

After the cleaning process, the fabricated pocket on the PMMA substrate was placed on the measuring stage of the goniometer (see Fig. 3.3) to take a picture of the sessile drop on the machined surface of the substrate. Live images of sessile drops were taken by the camera (Prosilica GC, Cupertino, CA) in 2 seconds after a single droplet of water was placed on the substrate.

3.4 Capillary driven flow experiment procedure

A surfactant has two main parts: hydrophobic and hydrophilic, which serve as a functional group. Surfactant reduces the surface tension as the concentration of surfactant increases. The surface becomes saturated with surfactant molecules and micelles starts to form. This point was defined as critical micelle concentration (CMC). In this research, dioctyl sulfosuccinate sodium salt (97% AOT, Sigma-Aldrich, St. Louis, MO) was used as a surfactant. A surfactant of 0.35mol/litre would be added to 100 ml of DI water. However, it was found that the surfactant solution reached the critical micelle concentration (CMC) at 0.08 M at which the increase of concentration does not affect the surface tension.

Wetting phenomena of a water droplet on substrates were of crucial interest in our daily life. The wetting behavior depends on two factors, the chemical composition and the roughness of the machined surface. AOT surfactant helped to satisfy the Young's equation by allowing a solution that the effect of surface tension is negligible [68].

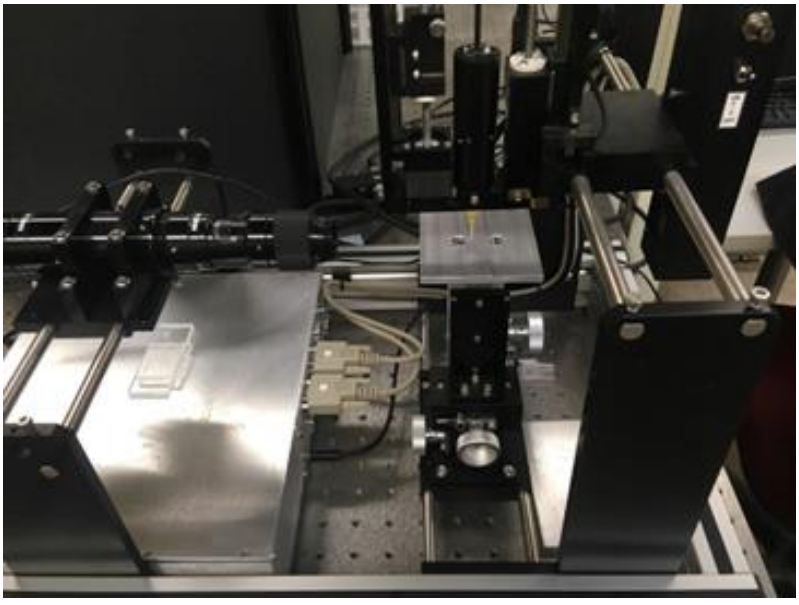

Fig 3.7: Contact Angle measurement setup

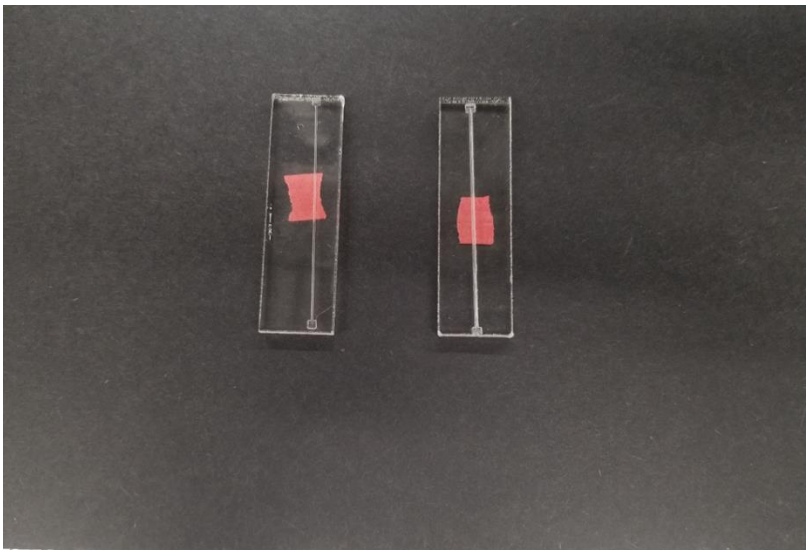

Fig 3.8: Microchannel samples.

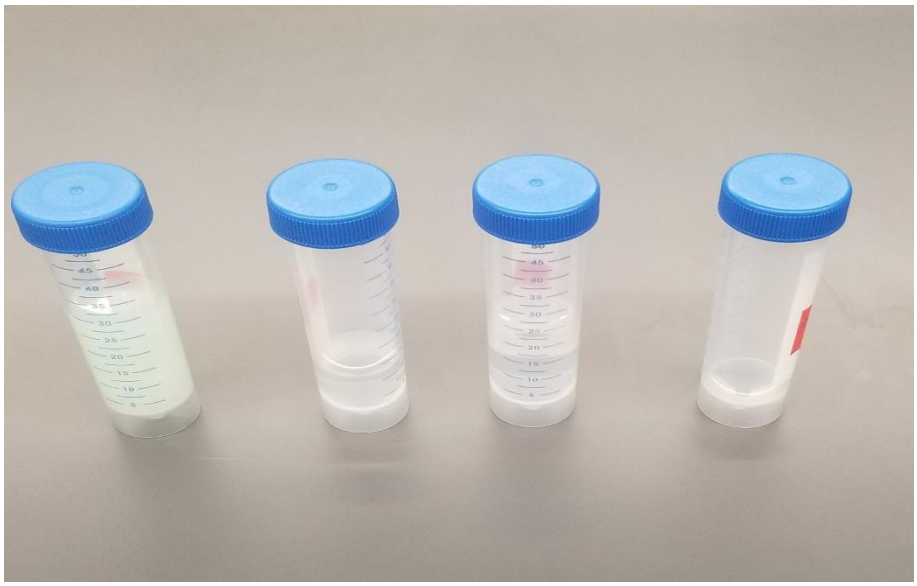

Fig 3.9: Test solutions of DI water-AOT mixture

3.5 AOT, dioctyl sulfosuccinate sodium salt

As stated with the Washburn equation (see Eq. 2.12), surface tension is one of the parameters that affects capillary driven flow by reducing surface tension. Even though the viscosity of the test fluid plays a role, the effect of capillary action is more pronounced as the fluid flows through the rectangular microchannel [43]. For a fluid with high surface tension means higher driving force was needed for the fluid to flow through a microchannels. Varying the concentration of AOT in the AOT-water test solutions (see Table **3.2**), different fluid mixtures [69] (see eq. 3.1 and 3.2) were used to see the interaction between micro-milled microchannel surface. In the capillary driven flow experiment, the same width of microchannels ($444 \pm 5\mu m$) was used to maintain the similar property of the microchannel for all 3 different viscous fluids. The capillary flow rate can be controlled by varying either the channel width or the viscosity of liquid.

Table 3.2: A table showing AOT solute dissolved in water

Samples	Volume of Water (ml)	Mass of AOT in the mixture (g)	Molar Concentration (mol/dm^3)	Equivalent percentage of AOT in the mixture (%)
1	100	0.5	0.01125	10
2	100	1.0	0.02249	20
3	100	2.0	0.04499	40
4	100	3.0	0.06748	61

$$Amount(g) = molar\ conc. \times \left(\frac{444.56g}{mol}\right) of AOT \times 0.1 litre \qquad \text{eq 3.1}$$

$$Concentrattion\ in\ \% = 100\ \times \left(\frac{mass\ solute\ in\ g}{volume\ solution\ in\ mL}\right) \qquad \text{eq 3.2}$$

3.6 Image acquisition and processing

Water droplets were introduced in the entry of microchannel and the capillary driven flow was observed. Consecutive images of the flow have been taken for a certain time duration to study the characteristics of the flow. The frame rate was 60ms and the position of the meniscus has been observed along with 200 consecutive images. The scaling of the meniscus position was calibrated using millimeter scale and ImageJ (NIH, Bethesda, MD). For the image calibration, there was a need to take an image of the scale and to standardize the particular distance between two points using ImageJ software. Next, in the same focus and resolution, the meniscus's position was observed and measured using ImageJ.

3.7 Microchannel fabrication

Six different microchannels were fabricated based on the following parameters, width of 300µm, 450µm, 600µm, 300µm, 450µm and 600µm with the corresponding depth of 100µm, 100µm, 100µm, 300µm, 300µm, and 600µm, respectively, (see Table 3.3, Table 3.4). These combinations have the same channel length of 60 mm. The fabrication process carried out on PMMA substrates, which were laser cut into 80 mm by 30 mm substrate. The spindle speed of 20,000 RPM and feed rate of 800 mm/min were used for microfabrication process (see Table 3.3).

Table 3.3: A table showing different combinations of depth (D), width (W) and aspect ratio (P)

	Width 1 (300 mm)	Width 2 (450 mm)	Width 3 (600 mm)
Depth 1 (100 mm)	P = 3	P = 4.5	-
Depth 2 (300 mm)	P = 1	P = 1.5	-
Depth 3 (600 mm)	P = 1/2	-	-

3.8 CAPILLARY DRIVEN FLOW RATE

Capillary driven flow experiments were carried out using a high-speed camera placed vertically at the focal length from the microchannel that was fabricated on a PMMA substrate (see fig 3.10, Table 3.4). The meniscus position, *x* was measured in the channel (see Appendix Table 4.3 – Table 4.8). The Washburn model (see eq. 2.12, eq. 3.3.) was used to consider the aspect ratio of microchannel (*P*), width (*W*) and depth (*D*) of microchannel, mobility parameter (*K*), contact angle (θ), the radius (*R*) of microchannel, the viscosity of fluid (μ), and time (*t*).

$$K = \frac{2\gamma D}{\mu}\frac{[2cos\theta - (1 - cos\theta)p)}{P^2}g(p) \qquad \text{eq. 3.3}$$

Surface tension (γ) and contact angle (θ) are measured. The software ImageJ was used for the digital image processing to see the capillary flow rate. Live record of the water flowing in the channel as a result of capillary forces was taken (see appendix Table 4.3 – Table 4.8). Also, the software records the time taken for the capillary to travel across the microchannel. Surface tension in test fluids affects capillary driven flow. Higher surface tension fluids require more force to work against the flow resistance.

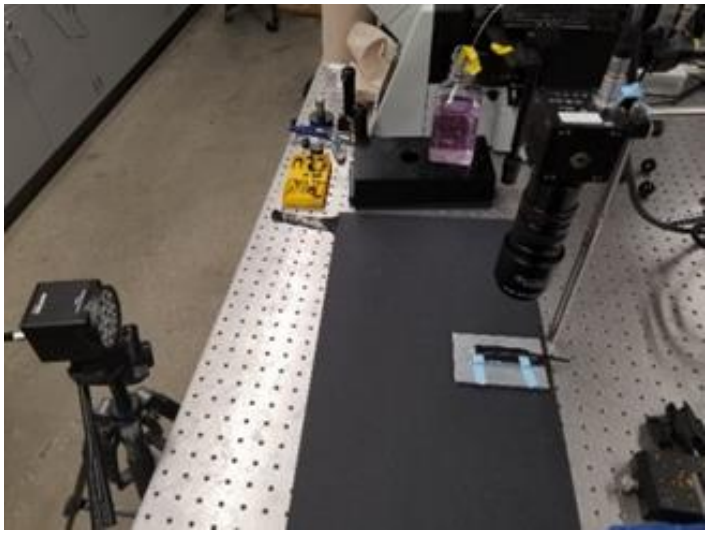

Fig 3.10: A picture showing the experimental setup of capillary driven flow experiment

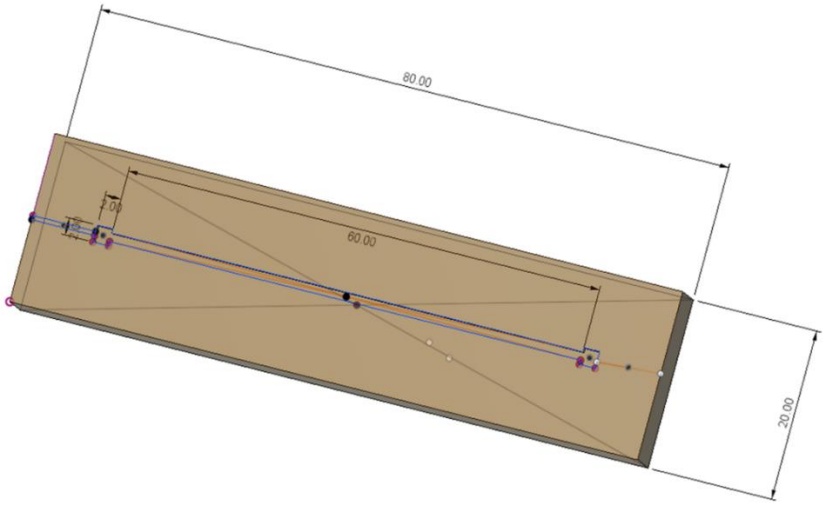

Fig 3.11: 3D CAD model for the microchannel used in capillary driven flow experiment

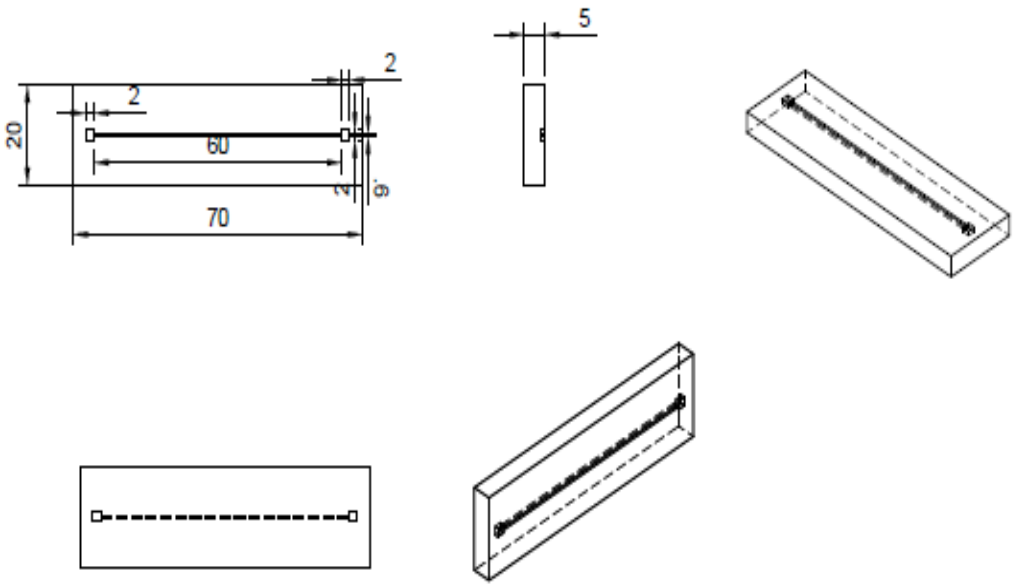

Fig 3.12: 2D Exploded view of the microchannel.

Table 3.4: A table showing the fabrication parameters combinations

	Speed (RPM)	Feed (mm/min)	Depth (µm)	Width (µm)	Length (mm)
1	20000	800	100	300	60
2	20000	800	100	450	60
3	20000	800	100	600	60
4	20000	800	300	300	60
5	20000	800	300	450	60
6	20000	800	600	730	60

CHAPTER 4

4.1 Surface roughness results and discussion

Surface roughness was one of the most important process outputs, but difficult to be analyzed due to the fact that it was a stochastic process due to uncertainties. This stochastic behavior become more dominant as tool diameter decreased. In our case, two main drilling bits of 101 μm to 203 μm diameters were used. A total of 54 samples were micro-milled with the first 27 samples milled with a milling bit of 101 μm and 27 samples were milled with a milling bit of 203 μm forming a reservoir to determine the surface quality in terms of the root mean square (RMS) value of surface roughness, Sq_{rms} and the average surface roughness, Sy using the profile-meter.

RMS of surface roughness were ranged between 0.14 μm to 3.7 μm. Table 4.1 shows the combinations of fabrication parameters based on Taguchi method, by holding a parameter constant and varying other parameters. Other parameters were also counted such as step-over diameter (20% of diameter of the milling bits) and two milling bits size of 101 μm and 203 μm diameters.

Table 4.1: Different levels of fabrication parameters including depth of cut, feed-rate and, spindle speed used in the experiments

FACTOR	LEVEL 1	LEVEL 2	LEVEL 3
A: Spindle Speed (N) (rpm)	10000	15000	20000
B: Feed Rate (F) (mm/min)	300	600	800
C: Depth of Cut (DOC) (μm)	50	75	150

One goal of the experiments was to reduce the surface roughness by variating the fabrication parameters, however, from the experimental results, this did not prove to be entirely true (Table **3.1**). For the first nine samples 1 to 9 (see Table 3.1 and 4.1), reducing the feed rate and depth of cut led to a significant decrease of the surface roughness, but the last three samples did not show the same trend (see fig 4.1.). The next 9 samples (samples 10 to 18) had a similar case with the first nine samples when the spindle speed was changed from 10,000 rpm to 20,000 rpm.

10,000 rpm

A. 101 µm diameter drilling bit

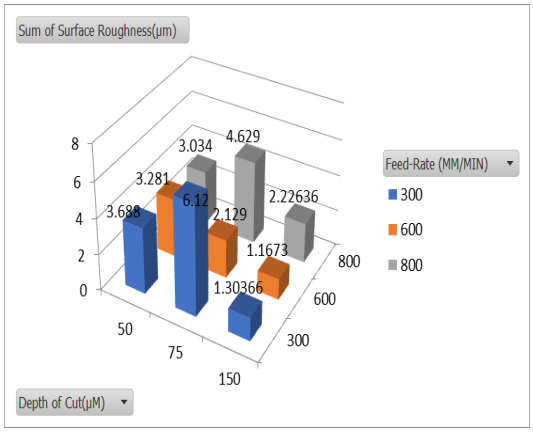

B. 203 µm diameter drilling bit

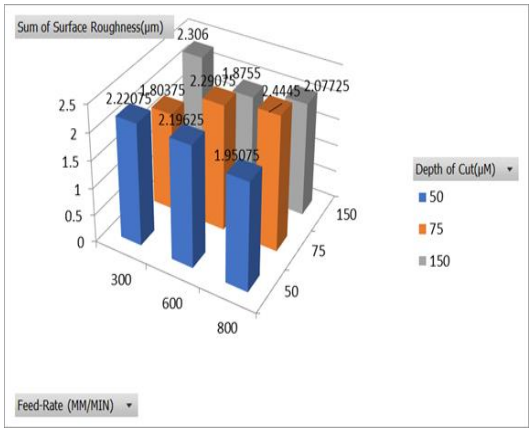

20,000 RPM

C. 101 µm diameter drilling bit

D.203 µm diameter drilling bit

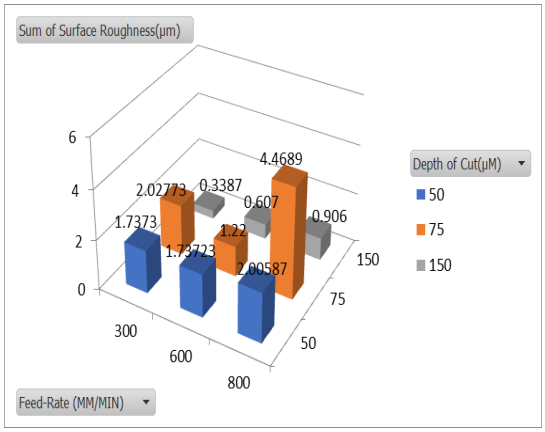

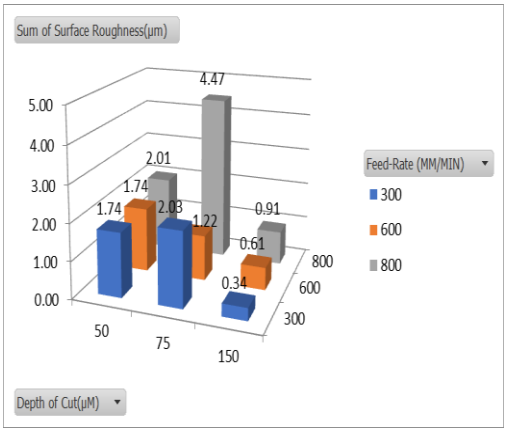

E. Depth of cut 50µm F. Depth of cut 75µm G. Depth of cut 150µm

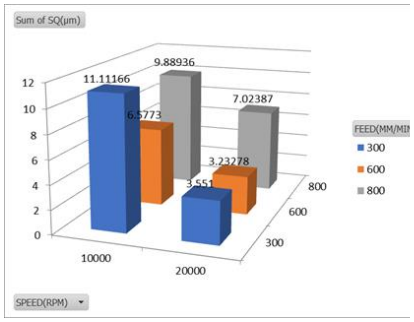

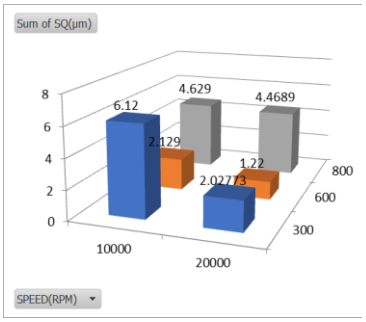

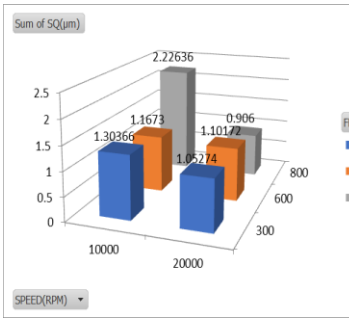

Fig 4.1: 3D bar plots showing variating feed-rates, surface roughness, depth of cut by fixing spindle speed and milling bit.

The changes in surface roughness were significantly higher compared to the second nine samples (samples 10 to 18) especially with an increase in feed-rate showing the highest surface roughness of about 4.11 µm. For the next nine samples (samples 19 to 27), the surface roughness increased with the depth of cut and feed rate, but not in progressive manner, which was like the first two groups (Samples 1 – 9 and 10 – 18) (see Fig. 4.0 E-2G). 28 out of the samples had a low surface roughness compared to the other 5 samples with surface roughness above 1.9 µm. Therefore, the overall results showed that surface

roughness varied and not consistent with the other experimental work as shown in literature [70] (see the appendix Fig 4.1.4).

4.2 Factor analysis

Factor analysis helps identifying which fabrication parameter has the highest impact on the surface roughness of machined PMMA substrate. The key fabrication parameters were combined to determine its effect on the surface roughness of the polymer (see Table 4.1 and 4.2). Table 4.2 shows the signal to noise ratio (S/N) where n = 4 for four times of roughness measurements and y^2_i is the sum of four times of roughness measurements. The table shows the different S/N ratio for each sample to quantify the impact of each fabrication factor on the surface roughness.

The results from the table show that the average surface roughness (Ra) values were inversely proportional to the average S/N ratios. The difference between the highest and lowest average S/N ratio of each factor was shown (see Table 4.2). A larger range indicates that the corresponding factor has a more pronounced effect on the surface quality of the micro-milled PMMA substrate. Factor C has the largest range (3.295) showing that the depth of cut has the greatest impact on surface quality. Factor B presents the smallest range (1.848) indicating that feed rate has the least impact on surface quality (see appendix 2.0 – 2.3). From the table, the combination showing the lowest surface roughness values of 0.14 μm and the S/N ratio of 14.458 was No. 26, which corresponds to the spindle speed of 10,000 RPM, the feed rate of 600 mm/min, and the depth of cut of 150 μm.

Table 4.2: Factor showing S/N results to determine the key cutting parameter

FACTORS	A (Spindle speed)	B (Feed Rate)	C (Depth of Cut)
Level 1	5.294	6.198	5.697
Level 2	6.377	7.408	5.157
Level 3	7.524	5.559	8.452
Range	2.230	1.848	3.295
Rank	2	3	1

4.3 Wettability studies

Wettability of the micromachined surface was of importance to check for the behavior of fluid when dispersed on it. Wenzel model was used to determine the relationship between contact angle and surface roughness where θ_e is the apparent contact angle, θ_y is the equilibrium contact angle, and r is the roughness value (see eq. 2.7). Wenzel suggested that the surface roughness factor amplifies the wettability of a surface. The hydrophilic surface becomes more hydrophilic, while a hydrophobic surface becomes more hydrophobic when the surface roughness increases.

From the experimental results, for the first nine samples (sample 1 to 9) (see Table 3.1), the contact angle reduces significantly as the surface roughness reduces, but there were peak values from samples 5 to 8, then the trend of decreasing continues from the sample nine.

10,000 (rpm)

20,000 (rpm)

DOC 50 mm

A

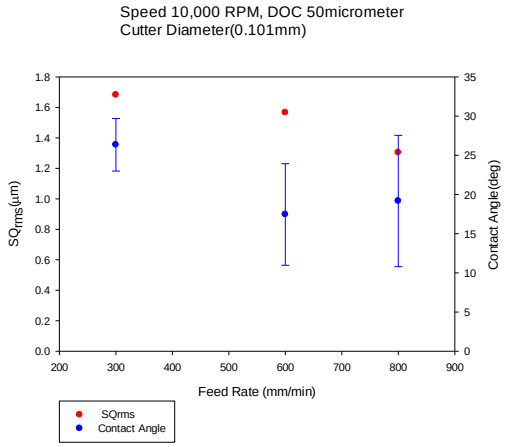

B

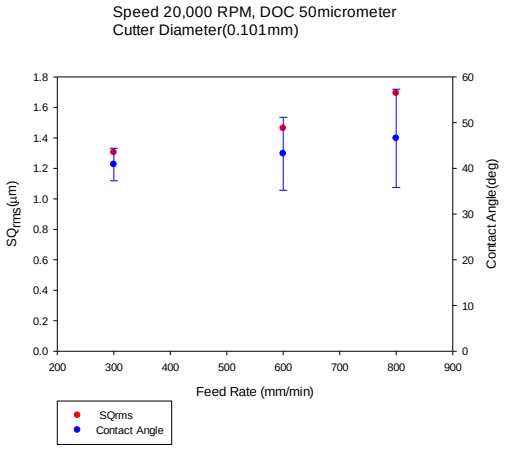

DOC 75 mm

C

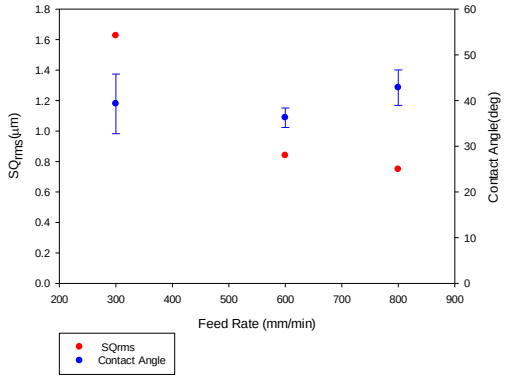

D

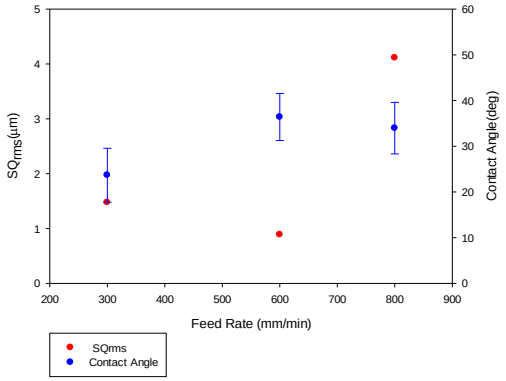

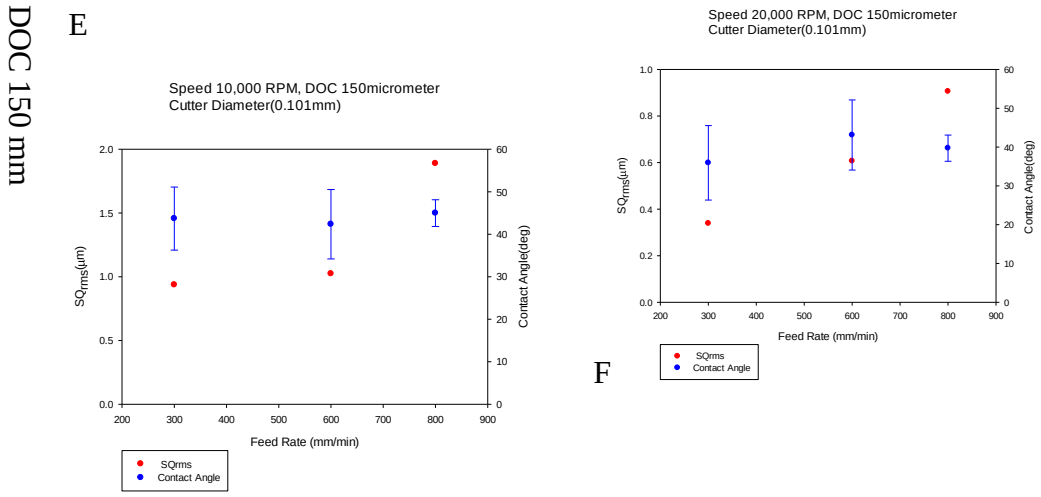

Fig 4.2: Measured contact angle based on the fabrication parameters especially milling bits 101 µm including spindle speed, feed-rate, and depth of cut. A to F show the measured contact angle in terms of feed-rate and, depth of cut based on the milling bits and spindle speed

For the next nine samples (Samples 19 to 27) (see Fig 4.2), the contact angle increased gradually, then decreased with the sample 23 and the slopes gradually down. Also, the same trend can be seen for the next six samples (samples 28 to 33). This resulted from a change in the depth of cut especially at 75 µm. Also, from the experimental results (see Table 3.1), most samples with surface roughness lower than 2.0 µm has contact angles lower than 55°. The result supports the Wenzel model, although there were some outliers especially at 75µm.

10,000 (rpm)

20,000 (rpm)

DOC 50 mm

A

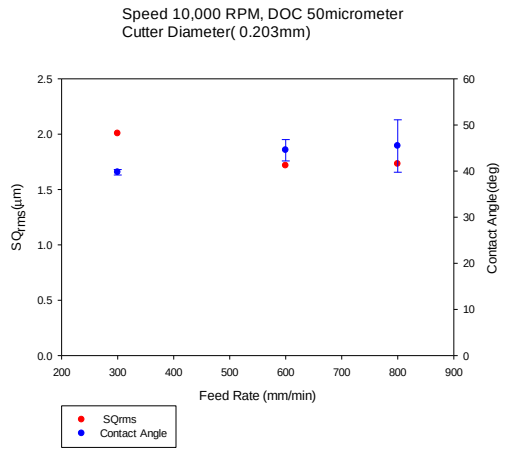

B

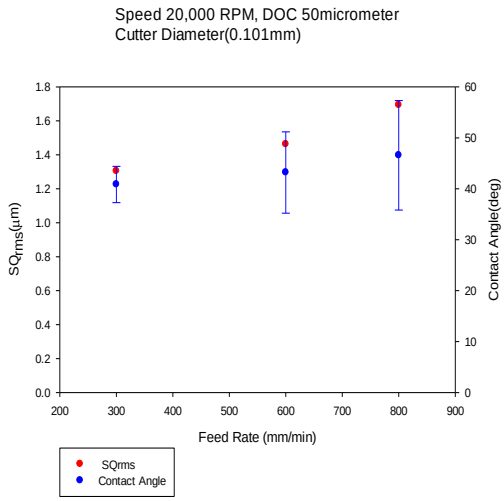

DOC 75 mm

C

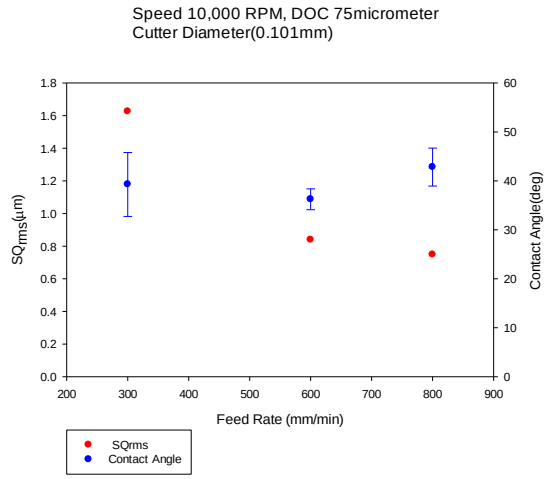

D

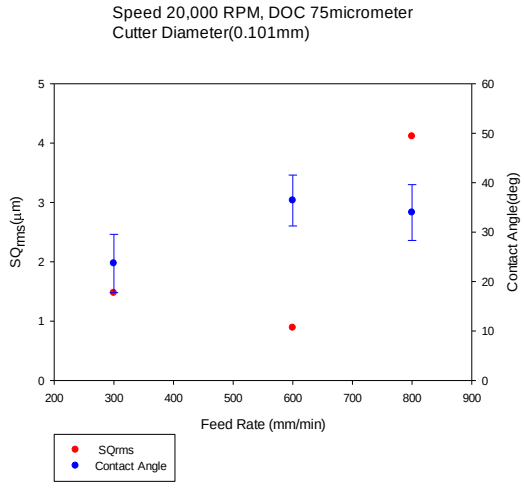

DOC 150 mm

E

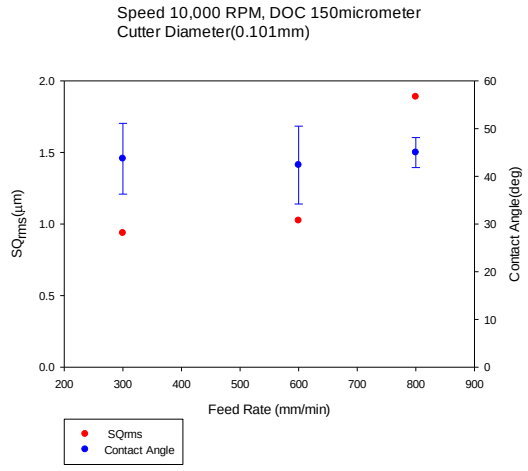

F

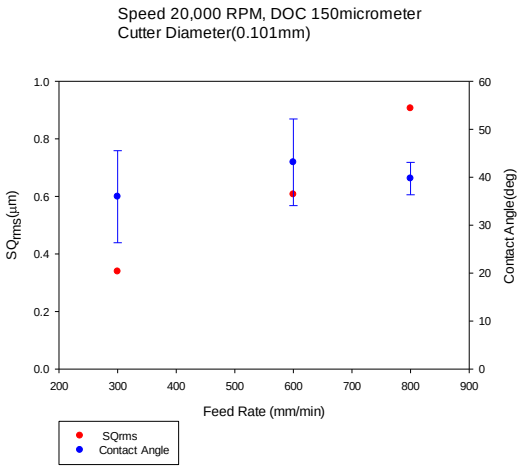

Fig 4.3: Measured contact angle based on the fabrication parameters especially milling bits 203 µm including spindle speed, feed-rate, and depth of cut. A to F show the measured contact angle in terms of feed-rate and, depth of cut based on the milling bits and spindle speed

DOC 50 µm

DOC 75 µm

DOC 150 µm

10,000 (RPM)

A

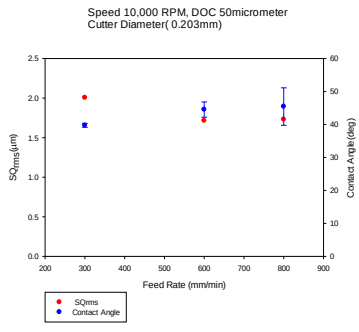

B

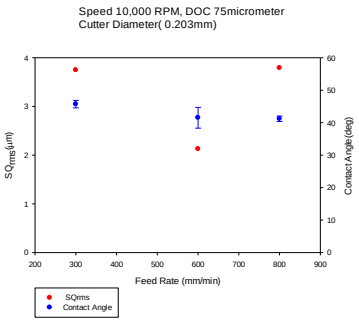

C

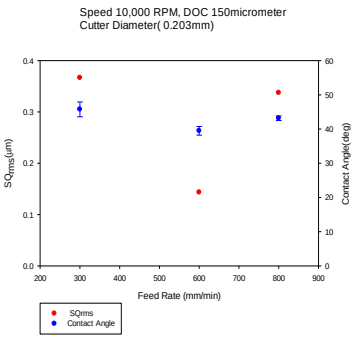

20,000 (RPM)

D E

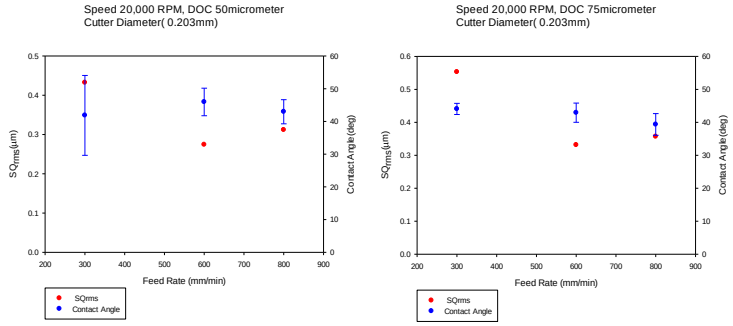

Fig 4.4: Measured contact angle based on the fabrication parameters especially milling bits 203 µm including spindle speed, feed-rate, and depth of cut. A to E show the measured contact angle in terms of feed-rate and, depth of cut based on the milling bits and spindle speed

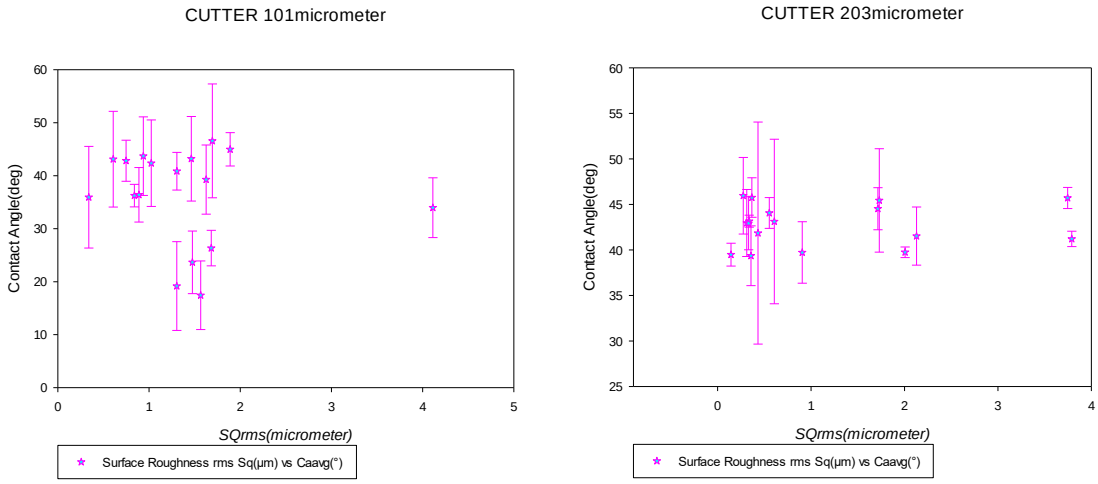

Fig 4.5: Measured contact angle versus surface roughness based on the milling bits

4.4 Capillary forces

Capillary driven flow occurs in a microchannel based on the effects of surface tension, therefore the speed can be modified by the surface properties of the microchannel, especially with surface wettability. From the physical theory, the attractive force between similar molecules known as cohesive force has a large impact on the surface tension. Although, the force between the dissimilar molecules was known as the adhesive force.

Surface tension arises in between the surface molecules due to the cohesive force. PMMA has an intrinsic property of being hydrophilic, therefore the adhesive force was strong while the cohesive force reduces the surface energy and turns the meniscus to be in concave shape. The Newton law of balance stabilizes both forces i.e., cohesive and adhesive forces. This force balance depends on surface wettability and drives the liquid in forward direction.

4.5 Capillary flow rate

$$x^2 = \frac{\gamma R cos\theta}{2\mu} t \qquad \text{eq. 4.1}$$

$$P = \frac{W}{D} \qquad \text{eq. 4.2}$$

$$F = \frac{2.5(B-600)+10(150-B_i)}{450} \qquad \text{eq. 4.3}$$

Eq. 4.1 shows the model used to measure the distance of travelling meniscus in a cylindrical channel as described by Washburn equation. However, in our case, a rectangular channel was considered where p is the aspect ratio, w is the width, d is the depth, k is the mobility parameter, θ is the contact angle, R is the radius, μ is the viscosity of fluid, and t is the time. Therefore, a model should be developed for this geometry, so as to measure the mobility parameter.

The main determinants of mobility parameters were width, diameter, aspect ratio, contact angle, and average flow velocity. However, eq. 4.2 shows that the width has more prominence in affecting the mobility parameter which is more evident in the experimental results (see Table 4.3). Using Taguchi method, we could have a pool of combined fabrication parameters. For the purpose of this experiment, six samples are considered because of the followings,

- As the aspect ratio decreases, the mobility parameter decreases and leads to

simultaneous reduction of squared position (x^2) (see eq. 4.2)

- Also based on the drilling bit size (101 µm & 203 µm)
- From Papautsky et al. (1999), Peng et. al. (1994), and Pfahler et al. (1991), certain width and depth were used to design rectangular channels [71]. This size serves as an extrapolation limit (see eq. 5).
- The following width were selected based on Papautsky, Peng and Pfhaler findings; 300 µm, 450 µm and 600 µm.

4.6 Capillary flow rate results and analysis

The overall results for the capillary flow rate complied with the Washburn equation (see appendix Table **4.3** to **4.8**). It was found that the capillary flow rate increased as the aspect ratio decreased after measuring the fluid meniscus using the image processing method. Also, from the graphs plotted, there was a linear relationship between the squared meniscus position of the fluid and time excepting when the mixture was at critical micelle concentration (3g), the capillary flow rate behaved abnormally by reducing its speed. Also, from the experimental results, the capillary flow rate decreased as the aspect ratio increased as predicted by Washburn model (see Table 5.1 to 5.6). The trendline for the experimental results corresponded to the results obtained from calculated results, which validated the fact that the overall results following the Washburn model (see Fig. 4.6.)

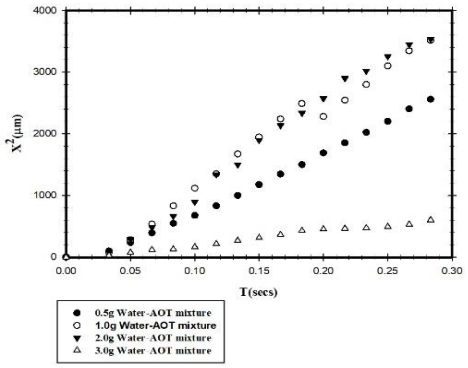

Fig 4.6: Graph showing experimental results for the meniscus position against time travelled in Sample A1

CHAPTER 5

5.1 Conclusion

From the overall experiments, the factor analysis showed that the depth of cut has a larger influence as a fabrication parameter compared to other parameters such as the spindle speed and the feed rate. Also, the wettability study showed that the spindle speed of 20,000 RPM, the feed rate of 800 mm/min, and the depth of cut of 150 mm/min were the optimum fabrication parameters in machining the microchannel on the PMMA substrate. The corresponding surface roughness resulted from the selected optimum fabrication parameters were 0.837μm, which met the requirement to create a microchannel, so that we could have a hydrophilic surface making it suitable for the proposed application. The corresponding surface roughness gave a contact angle of an equivalent of 30° signifying that the surface is hydrophilic. The wettability studies showed that the experimental results agreed with the Wenzel equation even though there was a certain level of inconsistencies. From the initial hypothesis, contact angles were supposed to decrease as the surface roughness increased, but this was not the case with this experiment which might be because of an inhomogeneity such as pores or cracks across the material surface. It could be another reason that surface roughness measurement is stochastic in nature due to the contact angle hysteresis and the evaporation rate during measurements.

The study on the capillary driven flow revealed that the capillary flow rate was at its optimum with the design parameter of aspect ratio of 1.23, width of 700μm and depth of 600μm. The capillary driven flow has the relatively fast in all the 6 samples and 3 mixture combinations (0.5g, 1.0g, and 2.0g) except for 3g. The speed is relatively low because the concentration of AOT was higher than 0.08M, which is the RCMC. The capillary driven

flow results showed complying with the Washburn model.

APPENDIX SECTION

1.0 G-CODES FOR MICROMILLING PROCESS

```
(1001)
(PMMADOC150.3MML1B1)
(T3 D=0.203 CR=0. - ZMIN=-0.15 - FLAT END MILL)
G90 G94 G91.1 G40 G49 G17
G21
G28 G91 Z0.
G90
(2D ADAPTIVE5)
M5
M9
T3 M6
S10000 M3
G54
M8
G0 X-31.628 Y20.555
G43 Z15. H3
Z5.
Z-0.034
G1 Z-0.055 F300.
X-31.623 Y20.551 Z-0.069
X-31.61 Y20.544 Z-0.075
G3 X-30.103 Y20.101 I1.618 J2.721
G1 X-30.091
X-30.088 Y20.102
X-30.053 Y20.151
X20.119 Y-22.717 Z-0.144
X20.122 Y-22.722 Z-0.13
G0 Z15.
M9
G28 G91 Z0.
G28 X0. Y0.
M30
```

```
(70000)
(PMMADOC150.3MML1B1)
(T1  D=0.101 CR=0. - ZMIN=-0.2 - FLAT END MILL)
G90 G94 G91.1 G40 G49 G17
G21
G28 G91 Z0.
G90

(2D POCKET3)
M5
M9
T1 M6
S1000 M3
G54
M8
G0 X-30.078 Y0.237
G43 Z15. H1
Z5.
G1 Z2.51 F1000.
X-30.087 Y0.236 Z2.5
X-30.114 Y0.244 Z2.499
X-30.131 Y0.265 Z2.498
X-30.134 Y0.293 Z2.497
X-30.122 Y0.317 Z2.496
X-30.098 Y0.331 Z2.495
X-30.071 Y0.329 Z2.494
X-30.049 Y0.313 Z2.493
X-30.039 Y0.288 Z2.492
X-30.045 Y0.261 Z2.491
X-30.065 Y0.242 Z2.49
X-30.092 Y0.237 Z2.489
X-30.117 Y0.247 Z2.488
X-30.133 Y0.27 Z2.487
Y0.297 Z2.486
X-30.119 Y0.32 Z2.485
```

```
X-32.021 Y2.112
X-32.002 Y2.148
X-31.974 Y2.176
X-31.938 Y2.195
X-31.898 Y2.201
X28.724
X28.764 Y2.195
X28.8 Y2.176
X28.828 Y2.148
X28.847 Y2.112
X28.853 Y2.072
Y-1.549
X28.847 Y-1.589
X28.828 Y-1.625
X28.8 Y-1.654
X28.764 Y-1.672
X28.724 Y-1.679
X24.04
X24.032 Y-1.684
X24.024 Y-1.688
X-32.037
Y2.211
X28.862
Y-1.688
X24.024
X24.015 Y-1.684 Z-0.19
G0 Z15.

M9
G28 G91 Z0.
G90
G28 G91 X0. Y0.
G90
M30
```

Table 1.0: A table showing capillary flow versus AOT-water mixture for sample A1

SAMPLE A1										
0.5G		1G		2G		3G		P (W/D)	W(μm)	D(μm)
X^2(μm)	t(secs)	X^2(μm)	t (secs)	X^2(μm)	t(secs)	X^2(μm)	t(secs)	3	300	100
0	0	0	0	0	0	0	0	3	300	100
99.08	0.033	74.77	0.03	84.23	0.033	29.87	0.03	3	300	100
236.93	0.05	280.74	0.05	288.12	0.05	76.12	0.05	3	300	100
392.69	0.067	536.04	0.07	480.76	0.067	119.61	0.07	3	300	100
548.03	0.08	831.12	0.08	664.58	0.083	129.40	0.08	3	300	100
675.66	0.1	1117.12	0.1	894.48	0.1	165.14	0.1	3	300	100
832.26	0.12	1351.64	0.12	1339.92	0.117	213.95	0.12	3	300	100
999.67	0.13	1673.5	0.13	1498.85	0.133	269.03	0.13	3	300	100
1175.82	0.15	1949.13	0.15	1898.98	0.15	314.24	0.15	3	300	100
1345.91	0.17	2240.04	0.17	2137.94	0.167	363.97	0.17	3	300	100
1498.73	0.18	2491.12	0.18	2337.52	0.183	428.47	0.18	3	300	100
1690.08	0.2	2280.80	0.2	2573.85	0.2	453.59	0.2	3	300	100
1852.97	0.22	2545.81	0.22	2900.08	0.217	465.43	0.22	3	300	100
2023.34	0.23	2799.69	0.23	3019.86	0.233	473.04	0.23	3	300	100

2201.21	0.25	3100.83	0.25	3256.23	0.25	492.83	0.25	3	300	100
2404.61	0.27	3346.44	0.27	3447.42	0.267	532.48	0.27	3	300	100
2560.92	0.28	3515.12	0.28	3534.14	0.283	602.67	0.28	3	300	100

Table 1.1: A table showing capillary flow versus AOT-water mixture for sample A2

SAMPLE A2										
0.5G		1G		2G		3G				
X^2(μm)	t(secs)	X^2(μm)	t(secs)	X^2(μm)	t(secs)	X^2(μm)	t(secs)	P (W/D)	W(μm)	D(μm)
0	0	0	0	0	0	0	0	4.5	450	100
1173.68	0.33	141.41	0.33	148.07	0.33	45.56	0.33	4.5	450	100
1137.97	0.35	300.09	0.35	382.94	0.35	124.51	0.35	4.5	450	100
1178.11	0.37	484.19	0.37	592.52	0.37	205.13	0.37	4.5	450	100
1195.52	0.38	778.49	0.38	767.87	0.38	259.51	0.38	4.5	450	100
1255.48	0.4	1031.34	0.4	1030.92	0.4	379.39	0.4	4.5	450	100
1295.87	0.42	1353.92	0.42	1292.16	0.42	460.19	0.42	4.5	450	100
1302.61	0.43	1627.73	0.43	1567.86	0.43	553.05	0.43	4.5	450	100
1327.53	0.45	1838.12	0.45	1830.10	0.45	649.94	0.45	4.5	450	100
1334.91	0.47	2138.42	0.47	2121.31	0.47	728.70	0.47	4.5	450	100
1348.62	0.48	2333.03	0.48	2360.32	0.48	811.69	0.48	4.5	450	100
1368.63	0.5	2640.97	0.5	2660.34	0.50	886.24	0.50	4.5	450	100
1389.42	0.52	2907.21	0.52	2867.28	0.52	973.79	0.52	4.5	450	100
1420.57	0.53	3081.24	0.53	3133.62	0.53	1045.16	0.53	4.5	450	100
1455.29	0.55	3303.65	0.55	3292.79	0.55	1119.86	0.55	4.5	450	100
1482.84	0.57	3577.90	0.57	3455.68	0.57	1208.50	0.57	4.5	450	100

Table 1.2: A table showing capillary flow versus AOT-water mixture for sample A3

SAMPLE A3										
0.5G		1G		2G		3G				
X^2(μm)	t(secs)	X^2(μm)	t(secs)	X^2(μm)	t(secs)	X^2(μm)	t(secs)	P (W/D)	W(μm)	D(μm)
0	0	0	0	0	0	0	0	6	600	100
55.31	1.02	269.60	1.02	73.87	1.02	185.42	1.02	6	600	100
110.85	2.02	336.93	2.02	132.12	2.02	235.78	2.02	6	600	100
172.65	3.02	601.80	3.02	227.20	3.02	373.13	3.02	6	600	100
245.09	4.02	806.47	4.02	380.78	4.02	497.80	4.02	6	600	100
326.48	5.02	1059.63	5.02	631.58	5.02	705.41	5.02	6	600	100
400.21	6.02	1326.11	6.02	914.63	6.02	861.96	6.02	6	600	100
456.25	7.02	1622.38	7.02	1216.97	7.02	991.17	7.02	6	600	100
537.96	8.02	1948.23	8.02	1523.80	8.02	1122.98	8.02	6	600	100
588.32	9.02	2193.89	9.02	1791.91	9.02	1249.46	9.02	6	600	100
650.46	10.02	2455.38	10.02	2027.63	10.02	1354.26	10.02	6	600	100
706.23	11.02	2751.20	11.02	2334.96	11.02	1485.14	11.02	6	600	100
758.01	12.02	2957.54	12.02	2525.54	12.02	1590.95	12.02	6	600	100
891.07	13.02	3314.66	13.02	2786.46	13.02	1724.69	13.02	6	600	100
991.90	14.02	3563.82	14.02	2963.53	14.02	1822.12	14.02	6	600	100
1085.63	15.02	3761.94	15.02	3109.55	15.02	1922.49	15.02	6	600	100

Table 1.3: A table showing capillary flow versus AOT-water mixture for sample A3

SAMPLE A4										
0.5G		1G		2G		3G				
X^2(μm)	t(secs)	X^2(μm)	t(secs)	X^2(μm)	t(secs)	X^2(μm)	t(secs)	P(W/D)	W(μm)	D(μm)
0	0	0	0	0	0	0	0	1	300	300
436.80	0.03	256.10	0.03	243.86	0.03	41.20	0.03	1	300	300
815.88	0.05	546.83	0.05	408.72	0.05	75.99	0.05	1	300	300
1271.74	0.07	922.82	0.07	620.48	0.07	117.24	0.06	1	300	300
1413.99	0.08	1285.10	0.08	835.70	0.08	164.89	0.08	1	300	300
1869.21	0.10	1369.12	0.10	1189.43	0.10	324.63	0.10	1	300	300
2126.13	0.12	1803.62	0.12	1557.80	0.12	345.64	0.12	1	300	300
2344.71	0.13	2003.31	0.13	2001.60	0.13	440.29	0.13	1	300	300
2542.98	0.15	2248.69	0.15	2405.30	0.15	565.04	0.15	1	300	300
2770.64	0.17	2399.48	0.17	2776.59	0.17	689.94	0.17	1	300	300
2924.27	0.18	2639.62	0.18	3164.49	0.18	761.92	0.18	1	300	300
3156.95	0.20	2768.72	0.20	3587.71	0.20	843.47	0.20	1	300	300

Table 1.4 A table showing capillary flow versus AOT-water mixture for sample A5

SAMPLE A5										
0.5G		1G		2G		3G				
X^2(μm)	t(secs)	X^2(μm)	t(secs)	X^2(μm)	t(secs)	X^2(μm)	t(secs)	P(W/D)	W(μm)	D(μm)
0	0	0	0	0	0	0	0	1.5	450	300
370.99	0.05	331.54	0.08	123.61	0.15	75.99	0.10	1.5	450	300
560.18	0.07	569.42	0.10	297.87	0.17	123.46	0.12	1.5	450	300
831.94	0.08	848.61	0.12	516.49	0.18	211.98	0.13	1.5	450	300
1203.30	0.10	1131.48	0.13	789.45	0.20	324.29	0.15	1.5	450	300
1589.06	0.12	1411.36	0.15	1093.59	0.22	432.09	0.17	1.5	450	300
2019.66	0.13	1786.19	0.17	1330.69	0.23	546.25	0.18	1.5	450	300
2435.46	0.15	2124.95	0.18	1062.15	0.25	591.94	0.20	1.5	450	300
2828.35	0.17	2473.81	0.20	1927.81	0.27	668.92	0.22	1.5	450	300
3218.03	0.18	2870.09	0.22	2170.43	0.28	740.03	0.23	1.5	450	300
3586.79	0.20	3229.67	0.23	2446.44	0.30	831.33	0.25	1.5	450	300
3808.18	0.27	3587.82	0.40	2720.15	0.28	870.45	0.23	1.5	450	300

Table 1.5: A table showing capillary flow versus AOT-water mixture for sample A6

SAMPLE A6										
0.5G		1G		2G		3G				
X^2(μm)	t(secs)	X^2(μm)	t(secs)	X^2(μm)	t(secs)	X^2(μm)	t(secs)	P(W/D)	W(μm)	D(μm)
0	0	0	0	0	0	0	0	1.23	730	600
445.06	0.05	1007.70	0.05	65.08	0.05	13.26	0.07	1.23	730	600
723.82	0.07	1410.28	0.07	90.52	0.07	41.24	0.08	1.23	730	600
1019.79	0.08	1821.98	0.08	331.83	0.08	82.89	0.10	1.23	730	600
1620.40	0.10	2267.68	0.10	476.13	0.10	130.04	0.12	1.23	730	600
1989.97	0.12	2741.79	0.12	645.42	0.12	182.65	0.13	1.23	730	600
2350.34	0.13	3173.73	0.13	901.51	0.13	238.18	0.15	1.23	730	600
2771.05	0.15	3602.32	0.15	1215.09	0.15	317.83	0.17	1.23	730	600

Sample A1

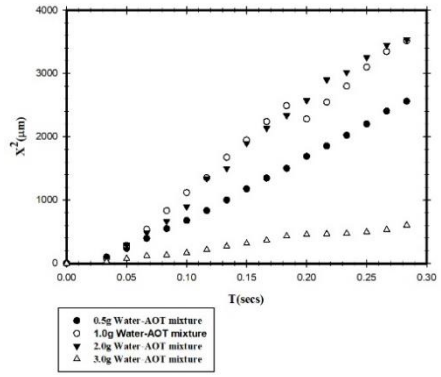

Sample A2

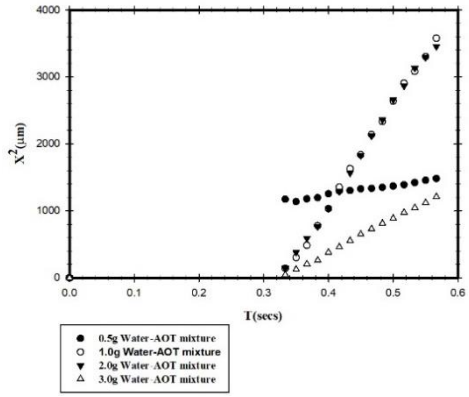

Sample A3

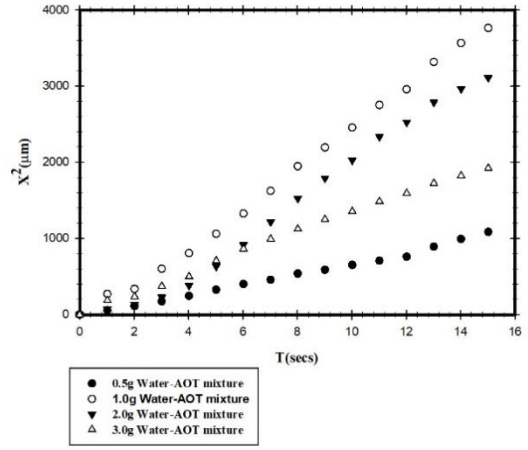

Sample A4

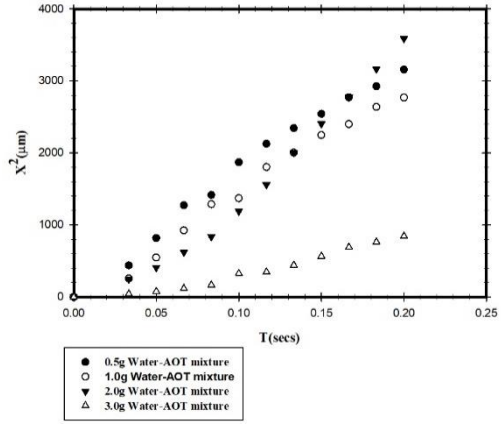

Sample A5

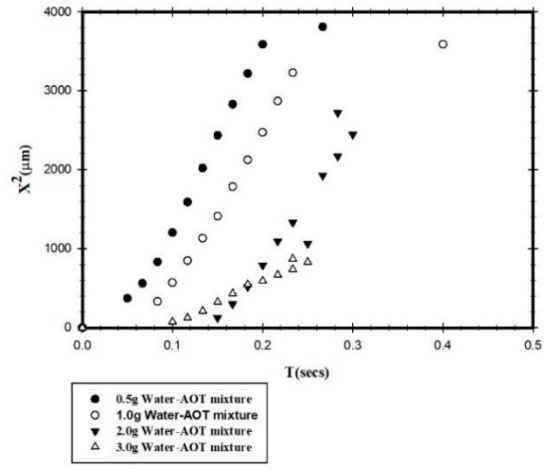

Sample A6

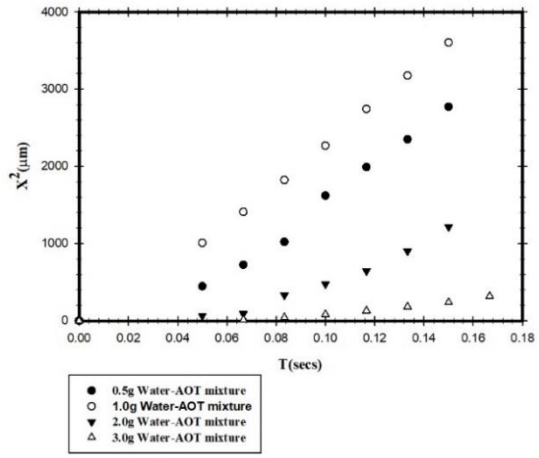

Fig 1.0: Graph plots A1 to A6 showing the different experimental capillary flow rate for different mass samples AOT-water mixtures

2.0 STATISCAL MODEL USED FOR DETERMINING THE SURFACE ROUGHNESS INCONSISTENCIES

$$R_a = a_0 . D_f^{a_1} . V^{a_2} . a_p^{a_3} . f_2^{a_4}$$

$$lgR_a = lga_0 . a_1 lgD_f . a_2 lgV . a_3 lga_p . a_4 lgf_2$$

From the equations above the following models was developed using R statical package:

Lm (log (Sm)`log (RPM) + log (Feed) + log (DOC) + log (Bit), data = Alo.reg) -> fit

Lm (log (Sm)`factor (ID), data=Alo.reg)-> fit.lof

Anova (fit, fit.lof)

Therefore, the two models based on the above algorithm;

Model 1: log (Sm)` log (RPM) + log (Feed) + log (DOC) + log (Bit)

Model 2: log (Sm)` log (Sm) ` factor (ID)

2.1 ANOVA RESULTS

Model 1: log (Sm) ~ log (RPM) + log (Feed) + log (DOC) + Log (Bit)

Model 2: log (Sm) ~ factor (ID)

Res. Df RSS Df s

Signif. Codes: 0*** 0.001** 0.01* 0.05. 0.1. 1.

Table 2.1.: A table showing the corresponding Anova results

	Res.Df	RSS	Df	Sum of Sq.	F	Pr.(>F)
1	211	2.5296				
2	162	1.2870	49	1.2426	3.1921	1.914e-08

2.3: P TEST

Signif. Codes: 0*** 0.001** 0.01* 0.05. 0.1. 1.
Residual standard error: 0.1095 on 211 degrees of freedom,
Multiple R-Squared: 0.2647,
Adjusted R-squared: 0.2508,
F-statistic: 18.99 on 4 and 211 DF, p-value: 2.351e-13

.

Table 2.2: A table showing the components contained in the mixture versus surface tension of the mixture

Components(mole/litre)	Surface tension with (0.08M) AOT (mN/m)
0.067	26.12+2.10
0.045	21.31+1.72
0.022	18.10+1.89
0.011	15.21+2.34

Table 2.3: A table showing the corresponding Anova results for different fabrication parameter

	Estimate Std.	Std. Error	T value	Pr(>|t|)
Intercept	6.15497	0.30762	20.008	<2e-16***
Log (RPM)	-0.19439	0.02620	-7.419	2.85e-12***
Log (Feed)	-0.05730	0.04827	-1.187	0.237
Log (DOC)	0.02952	0.04380	0.674	0.501
Log (Bit)	-0.09113	0.02134	-4.270	2.96e-05***

REFERENCES

1.Chen, Y., et al., Capillary driven flow in micro scale surface structures. Microelectronic Engineering, 2009. **86**(4-6): p. 1317-1320.

2.Teng, J.-t., et al., Fluid dynamics in microchannels, in Fluid Dynamics, Computational Modeling and Applications. 2012, Intechopen.

3.Wong, R. and H. Tse, Lateral flow immunoassay. 2008: Springer Science & Business Media.

4.Rapheal C. Wong, H.Y.T., Fluid Dynamics in Microchannel. Micro Process Engineering 2009: p. 3 - 10.

5.Tae Kyum Kim, S.W.O., Soon Cheol Hong, Young Joon Mok, and Eui Yui Choi, Point of care Fluorescence Immunoassay for Cardiac Panel Biomarkers. Journal of Clinical Laboratory Analysis, 2013. **28**: p. 419 - 427.

6.Songok, J. and M. Toivakka, Enhancing Capillary-Driven Flow for Paper-Based Microfluidic Channels. Acs Applied Materials & Interfaces, 2016. **8**(44): p. 30523-30530.

7.Size, M.M., Share & Trends Analysis Report by Application (Lab-on-a-Chip, Organs-on-Chips, Continuous Flow), By Technology (Medical, Non-Medical), By Material, And Segment Forecasts, 2020-2027. Grand View Research, 2020.

8.Wong, R.C., Lateral Flow Immunoassay.

9.Ma, Y., et al., Fabrication of super-hydrophobic film from PMMA with intrinsic water contact angle below 90. Polymer, 2007. **48**(26): p. 7455-7460.

10.Tsao, C.-W., Polymer microfluidics: Simple, low-cost fabrication process bridging academic lab research to commercialized production. Micromachines, 2016. **7**(12):

p. 225.

11.Foster, K. and G.A. Parker, Fluidics. 1970: Wiley-Interscience.

12.Humphrey, E.F. and D.H. Tarumoto, Fluidics. 1965: Fluid Amplifiers Associates.

13.Burton, G.W., A. Joyce, and K.U. Ingold, Is vitamin E the only lipid-soluble, chain-breaking antioxidant in human blood plasma and erythrocyte membranes? Archives of Biochemistry and Biophysics, 1983. **221**(1): p. 281-290.

14. M.D.B., Microfluidics Device helps Diagnose Sepsis. 2014.

15.Siegel, A.C., et al., Cofabrication of electromagnets and microfluidic systems in poly (dimethyl siloxane). Angewandte Chemie, 2006. **118**(41): p. 7031-7036.

16.Reyes, D.R. and H. van Heeren, Proceedings of the First Workshop on Standards for Microfluidics. Journal of Research of the National Institute of Standards & Technology, 2019. **124**(124001).

17.Gian Luca Morini, M.L., Experimental Analysis of Pressure Drop and Laminar to Turbulent Transition for Gas Flows in Smooth Microtubes. Heat Transfer Engineering, 2007.

18.Rascón, C., A.O. Parry, and D.G. Aarts, Geometry-induced capillary emptying. Proceedings of the National Academy of Sciences, 2016. **113**(45): p. 12633-12636.

19.Happel, J. and H. Brenner, Low Reynolds number hydrodynamics: with special applications to particulate media. Vol. 1. 2012: Springer Science & Business Media.

20.Vrentas, J., C. Jarzebski, and J. Duda, A Deborah number for diffusion in polymer-solvent systems. AIChE Journal, 1975. **21**(5): p. 894-901.

21.Kwack, E.-Y., Effect of Weissenberg number on turbulent heat transfer and friction

factor of viscoelastic fluids. 1983.

22.McKinley, G.H., Dimensionless groups for understanding free surface flows of complex fluids. 2005.

23.Dhiman, A., R. Chhabra, and V. Eswaran, Flow and heat transfer across a confined square cylinder in the steady flow regime: effect of Peclet number. International Journal of Heat and Mass Transfer, 2005. **48**(21-22): p. 4598-4614.

24.Gad-el-Hak, M., MEMS: Background and Fundamentals. 2005: CRC Press.

25.Rosendahl, U., A. Ohlhoff, and M.E. Dreyer, Choked flows in open capillary channels: theory, experiment and computations. Journal of Fluid Mechanics, 2004. **518**: p. 187.

26.Yetisen, A.K., M.S. Akram, and C.R. Lowe, based microfluidic point-of-care diagnostic devices. Lab on a Chip, 2013. **13**(12): p. 2210-2251.

27.Ichikawa, N., K. Hosokawa, and R. Maeda, Interface motion of capillary-driven flow in rectangular microchannel. Journal of colloid and interface science, 2004. **280**(1): p. 155-164.

28.Nunna, B.B., S. Zhuang, and E.S. Lee. Flow control mechanism of capillary driven flow in microchannel using non-mechanical forces. in APS Meeting Abstracts. 2016.

29.Speight, J.G., Asphalt materials science and technology. 2015: Butterworth-Heinemann.

30.Quake, S.a., Fluids Physics at the nanoliter scale. Review of Modern Physics, 2005. **77**.

31.Alting, L., et al., Micro engineering. CIRP Annals, 2003. **52**(2): p. 635-657.

32.Brousseau, E., S.S. Dimov, and D.T. Pham, Some recent advances in multi-material micro-and nano-manufacturing. The International Journal of Advanced

Manufacturing Technology, 2010. **47**(1-4): p. 161-180.

33.Zhang, X., et al., Cutting forces in micro-end-milling processes. International Journal of Machine Tools and Manufacture, 2016. **107**: p. 21-40.

34.Periyanan, P., U. Natarajan, and S. Yang, A study on the machining parameters optimization of micro-end milling process. International Journal of Engineering, Science and Technology, 2011. **3**(6): p. 237-246.

35.Chen, P.-c., An experimental study of micromilling parameters to manufacture microchannels on a PMMA substrate. Internal Journal Advance Manufacturing, 2014: p. 1623-1630.

36.Yang, D., et al., Dynamics of capillary-driven flow in open microchannels. The Journal of Physical Chemistry C, 2011. **115**(38): p. 18761-18769.

37.Hessel, V., et al., Micro Process Engineering, 3 Volume Set: A Comprehensive Handbook. Vol. 1. 2009: John Wiley & Sons.

38.Yih, C.-S., Kinetic-energy mass, momentum mass, and drift mass in steady irrotational subsonic flows. Journal of Fluid Mechanics, 1995. **297**: p. 29-36.

39.Huang, W., R.S. Bhullar, and Y.C. Fung, The surface-tension-driven flow of blood from a droplet into a capillary tube. Journal of biomechanical engineering, 2001. **123**(5): p. 446-454.

40.Irimia, D., R.G. Tompkins, and M. Toner, Single-cell chemical lysis in picoliter-scale closed volumes using a microfabricated device. Analytical chemistry, 2004. **76**(20): p. 6137-6143.

41.Irimia D., e.a., Single cell chemical lysis in picoliter scale closed volumes using a microfabricated device. Anal Chem, 2004: p. 6137-6143.

42.Kim, N., et al. Investigation of two-phase flow in rectangular micro-channels. in ASME 2008 Fluids Engineering Division Summer Meeting collocated with the Heat Transfer, Energy Sustainability, and 3rd Energy Nanotechnology Conferences. 2008. American Society of Mechanical Engineers.

43.De Gennes, P.-G., F. Brochard-Wyart, and D. Quéré, Capillarity and wetting phenomena: drops, bubbles, pearls, waves. 2013: Springer Science & Business Media.

44.Brydson, e.a., Plastics Material. 1989.

45.Campo, E.A., The Complete Part Design Handbook. 2006.

46.Osswald, e.a., International Plastics Handbook. 2006.

47.Strong, Plastics Materials and Processing. 2000.

48.Brydson, J.A., Plastics materials. 1999: Elsevier.

49.Dornfeld, D., S. Min, and Y. Takeuchi, Recent advances in mechanical micromachining. CIRP annals, 2006. **55**(2): p. 745-768.

50.Oliaei, S.N.B. and Y. Karpat, Experimental investigations on micro milling of Stavax stainless steel. Procedia CIRP, 2014. **14**: p. 377-382.

51.Biermann, D., et al., Manufacturing of dies from hardened tool steels by 3-axis micromilling. Production Engineering, 2011. **5**(2): p. 209-217.

52.Filiz, S., et al., An experimental investigation of micro-machinability of copper 101 using tungsten carbide micro-endmills. International Journal of Machine Tools and Manufacture, 2007. **47**(7-8): p. 1088-1100.

53.Yang, J.L. and J.C. Chen, A systematic approach for identifying optimum surface roughness performance in end-milling operations. Journal of industrial technology,

2001. **17**(2): p. 1-8.

54.Antony, J. and M. Kaye, Experimental quality: a strategic approach to achieve and improve quality. 2012: Springer Science & Business Media.

55.Montgomery, D.C., Design and analysis of experiments. 2017: John Wiley & sons.

56.Torng, C.-C., C.-Y. Chou, and H.-R. Liu, Applying quality engineering technique to improve wastewater treatment. Journal of Industrial Technology, 1999. **15**(1): p. 1-7.

57.Taguchi, G. and M.S. Phadke, Quality engineering through design optimization, in Quality Control, Robust Design, and the Taguchi Method. 1989, Springer. p. 77-96.

58.Athreya, S. and Y. Venkatesh, Application of Taguchi method for optimization of process parameters in improving the surface roughness of lathe facing operation. International Refereed Journal of Engineering and Science, 2012. **1**(3): p. 13-19.

59.Asiltürk, I. and M. Çunkaş, Modeling and prediction of surface roughness in turning operations using artificial neural network and multiple regression method. Expert systems with applications, 2011. **38**(5): p. 5826-5832.

60.K.J. Kubiak, e.a., Wettability versus roughness of engineering surfaces. Vol. 271. 2011: Wear.

61.Hurst, S.M., et al., A universally applicable method for fabricating superhydrophobic polymer surfaces. Colloids and Surfaces A: Physicochemical and Engineering Aspects, 2012. **407**: p. 85-90.

62.Prof. Dr. rer. nat. Andreas Tünnermann, e.a., Roughness, wetting, and optical properties of functional surfaces. 2013.

63.Influence of surface roughness on contact angle and wettability.

64.Kubiak, K., et al., Wettability versus roughness of engineering surfaces. Wear, 2011. **271**(3-4): p. 523-528.

65.Zhou, X. and J.T.M. De Hosson, Influence of surface roughness on the wetting angle. Journal of materials research, 1995. **10**(8): p. 1984-1992.

66.Khaleel, O.T., Selecting an optimal surfactant for use in EOR: an experimental study. 2017, Colorado School of Mines. Arthur Lakes Library.

67.Khaleel, O.T., Selecting an Optimal Surfactant for Use in EOR: An Experimental Study. 2017.

68.Emad Jafari Nodoushan, Y.J.L., Namwon Kim, Temperature and Salinity Effects on Rhelogical Characteristics of Wormlike Micellar Solution. 2019.

69.Hamraoui, A. and T. Nylander, Analytical approach for the Lucas–Washburn equation. Journal of colloid and interface science, 2002. **250**(2): p. 415-421.

70.Esteves, R., N. Onukwuba, and B. Dikici Ph D, Determination of surfactant solution viscosities with a rotational viscometer. Beyond: Undergraduate Research Journal, 2016. **1**(1): p. 2.

71.Anil, K., et al. Effect of cutting parameters on surface finish and machinability of graphite reinforced Al-8011 matrix composite. in IOP Conference Series: Materials Science and Engineering. 2017. IOP Publishing.